

Article

# Origin and Age Determination of the Neotethys Meliata Basin Ophiolite Fragments in the Late Jurassic–Early Cretaceous Accretionary Wedge Mélange (Inner Western Carpathians, Slovakia)

Marián Putiš<sup>1,\*</sup>, Ján Soták<sup>2</sup>, Qiu-Li Li<sup>3</sup>, Martin Ondrejka<sup>1</sup>, Xian-Hua Li<sup>3</sup> , Zhaochu Hu<sup>4</sup>, Xiaoxiao Ling<sup>3</sup>, Ondrej Nemeč<sup>1</sup>, Zoltán Németh<sup>5</sup> and Peter Ružička<sup>1</sup>

<sup>1</sup> Department of Mineralogy and Petrology, Faculty of Natural Sciences, Comenius University in Bratislava, 842 15 Bratislava, Slovakia; martin.ondrejka@uniba.sk (M.O.); ondrej.nemec@uniba.sk (O.N.); peter.ruzicka@uniba.sk (P.R.)

<sup>2</sup> Earth Science Institute, Slovak Academy of Sciences, 974 11 Banská Bystrica, Slovakia; sotak@savbb.sk

<sup>3</sup> State Key Laboratory of Lithospheric Evolution, Institute of Geology and Geophysics, Chinese Academy of Sciences, Beijing 100029, China; liqiuli@mail.iggcas.ac.cn (Q.-L.L.); lixh@gig.ac.cn (X.-H.L.); lingxx@mail.iggcas.ac.cn (X.L.)

<sup>4</sup> State Key Laboratory of Geological Processes and Mineral Resources, China University of Geosciences, Wuhan 430074, China; zchu@vip.sina.com

<sup>5</sup> State Geological Institute of Dionýz Štúr, 817 04 Bratislava, Slovakia; zoltan.nemeth@geology.sk

\* Correspondence: marian.putis@uniba.sk

Received: 1 July 2019; Accepted: 19 October 2019; Published: 23 October 2019



**Abstract:** This study reports the Neotethyan Meliata Basin ophiolite fragments in the Late Jurassic–Early Cretaceous accretionary wedge mélangé in the southern part of the Inner Western Carpathians (IWC). Here we present new lithostratigraphical, petrographical, geochemical, and geochronological data obtained from the mélangé blocks used to reconstruct the Meliaticum paleotectonic zones in a tentative evolutionary model of this accretionary wedge. The Dobšiná mélangé block continental margin carbonatic and siliciclastic sediments have calc-alkaline basalt intercalations. The basalt Concordia age dated to  $245.5 \pm 3.3$  Ma by U–Pb SIMS on zircon most likely indicates the pre-oceanic advanced early Middle Triassic continental rifting stage. The evolving marginal oceanic crust is composed of Middle to Upper Triassic cherty shales to radiolarites. The detrital zircon U–Pb SIMS Concordia ages of  $247 \pm 4$  Ma and  $243 \pm 4$  Ma from a cherty shale, and the xenocryst zircon population Concordia age of  $266 \pm 3$  Ma from a 0.5 m thick “normal” mid-ocean ridge (N-MOR) basalt layer in this cherty shale reveal the connection of the oceanic basin to the adjacent rifting continental margin. The chertified reddish limestone transition to radiolarite indicates syn-rift basin deepening. Upwards, regular alternating N-MOR basalts and radiolarites are often disturbed by peperite breccia horizons. The Nd isotope values of these basalts ( $\epsilon\text{Nd}_{240} = 7\text{--}8$ ) are consistent with their chondrite normalized rare earth element (REE) patterns and indicate a depleted mantle source. The Triassic ophiolitic suite also comprises rare ocean island (OI) basalts ( $\epsilon\text{Nd}_{240} = 5$ ) and serpentinitized subduction unrelated peridotites. The Middle to Late Jurassic shortening and southward intra-oceanic and continental margin subduction at approximately 170–150 Ma enhanced the formation of the trench-like Jurassic flysch succession which preceded the closure of the Meliata Basin. The flysch sediments form a mélangé matrix of olistolithic unsubsducted, obducted, and MP–HP/LT metamorphosed exhumed blocks of the Triassic to Lower Jurassic successions. Blocks of peridotites, rodingites, blueschists, greenschists, rare amphibolites, deep-water shaly sediments and shallow- to deep-water carbonates are typical members of the mélangé. The Meliatic accretionary wedge mélangé nappe outliers were incorporated in the IWC orogenic wedge in the late Early Cretaceous according to metamorphic rutile U–Pb SIMS ages of  $100 \pm 10$  Ma determined from a Jaklovce metabasalt.

**Keywords:** Neotethys; Meliatic accretionary wedge mélangé; Inner Western Carpathians; lithostratigraphy; petrography; geochemistry; geochronology

## 1. Introduction

The Middle Triassic–Late Jurassic oceanic Meliata Basin is part of the Neotethys Ocean [1–10]. Meliaticum of the Inner Western Carpathians (IWC; Figure 1) originated in a NW Neotethys oceanic and continental margin thus representing northern branch of this ocean. Paleogeographic schemes show that this Tethyan ocean formed the embayment between the Eurasian and Gondwanian parts of Pangea [6,10–14]. Some authors place the Meliata Basin as a back-arc basin (BAB) on the Late Permian rifted Eurasian active continental margin above a Paleotethys subduction zone [12,15–17], but others consider it formed during the rifting of the Neotethys passive continental margin [10].

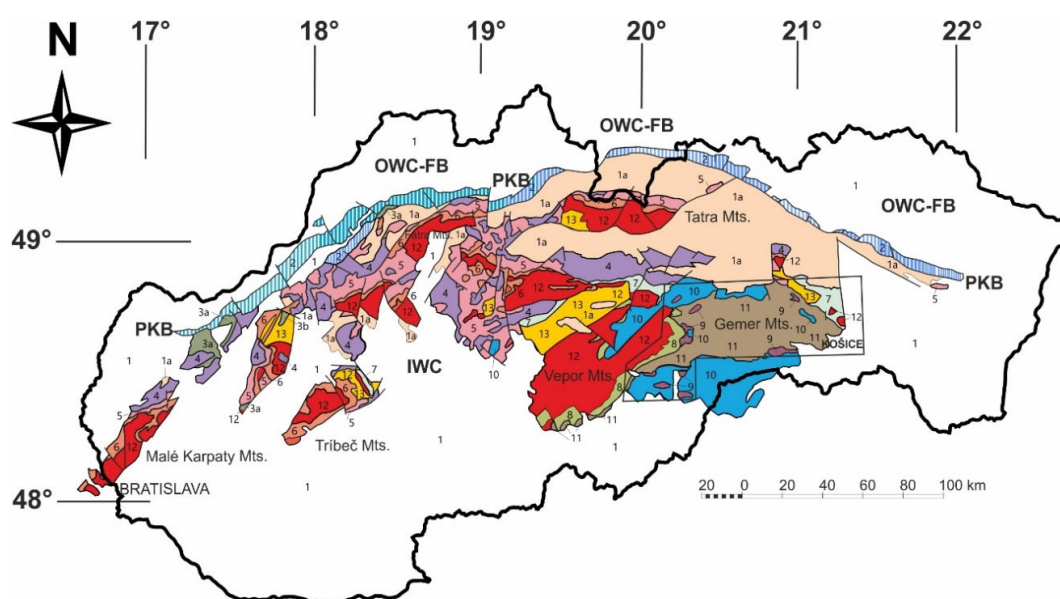


**Figure 1.** Schematic tectonic map of the Inner Western Carpathians (IWC, modified from [18]). 1—Quaternary and Cenozoic deposits undivided; Outer Western Carpathians Flysch Belt (OWC-FB); 1a—Paleogene deposits of the IWC; 2—Pieniny Klippen Belt (PKB); 3a—Upper Cretaceous to Eocene Gosau-type sediments; 3b—Upper Cretaceous Infratatic Succession; 4—Hronic nappes; 5—Fatric nappes; 6—Tatric cover; 7—North-Veporic cover; 8—South-Veporic cover; 9—Meliatic nappes; 10—Silicic nappes (including Turnaicum); 11—Gemic Paleozoic basement (Variscan Lower Unit) and cover; 12—Variscan Upper Unit; and 13—Variscan Middle Unit. The square area is depicted in more detail in Figure 2.

The IWC south of the Outer Western Carpathians Flysch Belt (OWC-FB) and the Pieniny Klippen Belt (PKB) comprise basement–cover complexes included in a north-vergency fold and thrust system (Figure 1). These are further subdivided from north to south and bottom to top into the Infratatic, Tatric, Veporic, and Gemic tectonic zones, separated by major Cretaceous shear zones [19–23]. The Meliata Superunit occurs as relatively small km-scale blocks or the north-vergency nappe outliers overlying the Gemic and southern part of the Veporic superunits which are inferred to have been part of the northern continental margin of the Middle Triassic to early Late Jurassic oceanic Meliata Basin [8,23]. The Pelso Superunit [6,11,24,25] could be an opposite southern continental margin of the western Neotethys embayment [8]). The Meliatic nappe outliers overlie the IWC orogenic wedge and are overlain in turn by the Turňa and Silica nappes [23].

The Meliaticum was reported to be an incomplete ophiolite suite composed of mid-ocean ridge basalts (MORBs) and serpentized peridotites associated with Middle Triassic pelagic carbonatic and cherty sediments [1,3,4,26,27]. The Permian to Middle Triassic continental margin sediments are associated with calc-alkaline basalts [5], and some of these underwent subduction metamorphism up to the blueschist facies [28–30] and became part of an accretionary wedge mélangé with the unmetamorphosed to lowest anchimetamorphosed Jurassic trench-like flysch sediments [8]. The Tornakápolna series of the Rudabánya Hills in northern Hungary (“Bódva Valley Ophiolite complex”) is considered to be as the mid-Triassic equivalent of the Meliata Unit in Slovak IWC [6,31–37]. The Bodva-Telekesvölgy Triassic–Middle Jurassic succession is overthrust there by Torna Series (Torna/Turňa Nappe) and by the Telekesoldal Jurassic sediments and Jurassic ophiolites. These ophiolites are equivalent of the Szarvaskő ophiolites in the Telekesoldal and Mónosbél nappes [37–39]. Meliatic type Triassic successions emplaced in Permian evaporitic mélangé were discovered also in the Northern Calcareous Alps in Austria [3,40–42].

Herein, we reconstruct the evolutionary stages of the Meliata Basin from the investigated dismembered Late Jurassic–Early Cretaceous mélangé blocks exposed in the IWC in order to test the formation of a marginal basin accretionary wedge. The major aim of this work is to define the principal paleotectonic zones of this basin, the rocks of which supplied the Meliatic accretionary wedge mélangé, with focusing on the ophiolitic remnants. The research methods in Chapter 3 then record the following applied investigations: A detailed field study of chosen lithological cross-sections, microscopic petrography, EPMA, XRF, ICP–OES, ICP–MS, TIMS, and SIMS U–Pb zircon and rutile dating. These determined the mineral chemical composition, the whole-rock chemistry including REE and Nd isotopes and detrital or xenocryst zircon isotopic ages. Finally, we employed biostratigraphic research of the inferred Middle Triassic cherty shales to radiolarites associated with basalts in a key Jaklovce cross-section and inferred Jurassic calcareous shales at Dobšiná.

Abbreviations of rock-forming minerals names used in the text, tables and figures are: Ab—albite, Act—actinolite, Amp—amphibole, Ap—apatite, Cal—calcite, Cel—celadonite, Chl—chlorite, Cpx—clinopyroxene, Czo—clinozoisite, Dol—dolomite, Ed—edenite, Ep—epidote, Gl—glaucophanes, Grt—garnet, Hbl—hornblende, H-Grs—hydro-grossular, H-Adr—hydro-andradite, Jd—jadeite, Kfs—potassium feldspar, Mag—magnetite, Mnz—monazite, Ms—muscovite, Cel-Ms—celadonite-rich Ms, Pg—pargasite, Phg—phengite (~Cel-Ms), Pl—plagioclase, Prg—pargasite, Prv—perovskite, Qz—quartz, Rbk—riebeckite, Rt—rutile, Spl—spinel, Tlc—talc, Tr—tremolite, Ttn—titanite, Tur—tourmaline, WhM—white mica, Win—winchite, Zrn—zircon.

## 2. Geological Setting

Geological maps [43,44] show that the Meliatic nappe outliers mostly overlie the Permian–Lower Triassic sedimentary cover of the IWC Gemic Superunit (Figure 2). The Gemic pre-Alpine basement preserves a Carboniferous suture after the closure of the Devonian part of the Paleotethys Ocean [21,45–48], and the suture zone is marked by thick Lower to Upper Carboniferous complexes including mélangé blocks of the exhumed MP to HP basement rocks [49,50]. The Neotethyan Meliaticum thus overlies such a suture marked by the Devonian N-MORBs of the Gemic basement Klátov Group [48]. The Variscan Gemic basement partly resembles the basement complexes of the Noric terrane in the Transdanubian Range, Dinarides, and Southern Alps [51,52].

The evolution of the Meliata Basin was preceded by the Permian to Early Triassic continental rifting stage. This time period is consistent with the Pangea super-continent break-up [12,15–17], and almost all the IWC units bear the signatures of this global extension event by distinct Permian magmatic activity. Calc-alkaline to alkaline acidic to basic volcanics, subvolcanics, lamprophyres, and some plutonic rocks were dated as Permian in the Infratatic [53], Tatic [54], Veporic [47,55,56], Gemic [57–59], Meliatic [58], and Silicic [60] superunits. Typical intra-plate continental tholeiites occur in a Permian succession of the Hronic Nappe [61] overlying the IWC Fatic, Tatic, and Infratatic nappes (Figure 1).

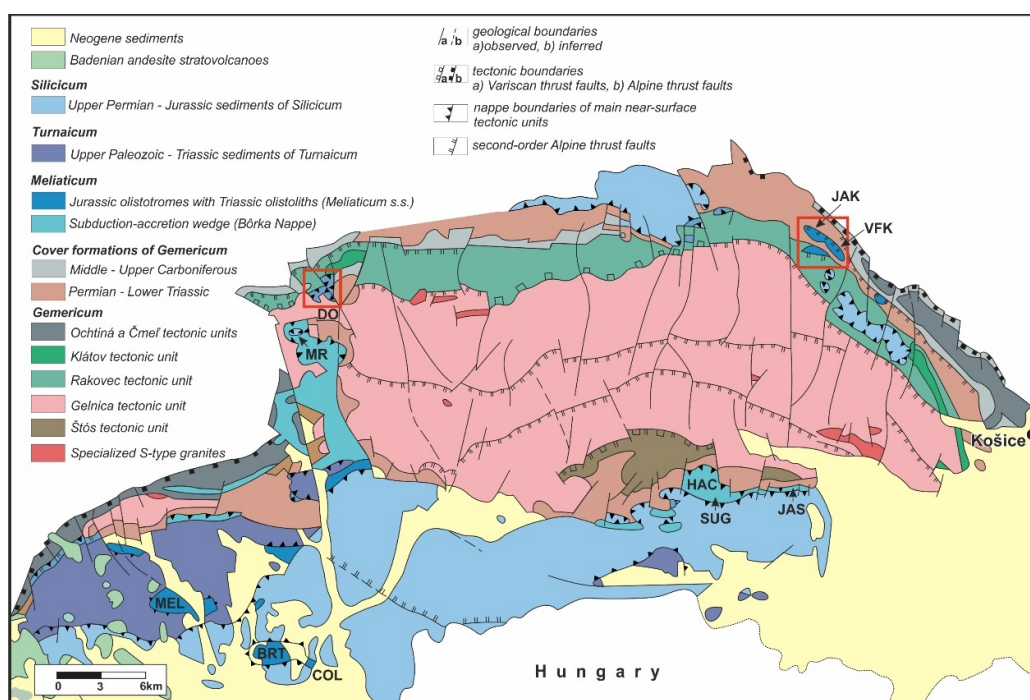


**Figure 2.** Tectonic map of the southeastern part of the IWC (modified from [43,44]). Red squares—investigated areas in greater detail at Dobšiná (DO), Jaklovce (JAK), and Veľký Folkmár (VFK). Additional samples are from Malý Radzim Hill near Brdárka (MR), Meliata (MEL), Bretka (BRT), Čoltovo (COL), Hačava (HAC), and Šugov Valley (SUG); and Jasov (JAS).

The Triassic–Jurassic oceanic crust fragments occur only in the Meliatic Late Jurassic–Early Cretaceous mélangé dismembered throughout the Gemericum. The Gemeric Superunit comprises Early Paleozoic basement complexes with the Carboniferous and Permian and subordinate Mesozoic cover rocks [62]. The Meliatic nappe outliers are overlain by the Turňa (in Slovakia)/Torna (in Hungary) Nappe [34,63,64], and the Turnaicum is composed of very low-grade to low-grade Upper Carboniferous, Permian, and Lower Triassic clastic sequences, lower Anisian platform carbonates and upper Anisian to Upper Triassic pelagic limestones and shales. These are partly imbricated with the underlying Meliatic complexes [34,40,63,65]. The uppermost tectonostratigraphic unit is the Silica Nappe [6,66] composed of Triassic–Jurassic successions, and this nappe system continues in the Aggtelek–Rudabánya Hills north of the Bükk Mountains and the Darnó line in Hungary [34].

The Meliatic nappe outliers include shallow-water platform Steinalm-type (Honce) carbonates of Anisian age and are followed upwardly by Ladinian and Upper Triassic to Lower Jurassic siliceous carbonates, with their age determined by conodonts [4]. The reddish (Žarnov) limestones of upper Anisian age are often present as neptunic dykes in pale platformal carbonates and these indicate the platform break-up and the Meliata Basin syn-rift stage [2,4]. A high five to seven color alteration index of conodonts is compatible with their marble character [67]. This succession at the Jaklovce village and nearby Kurtova skala Hill was classified as a mega-olistolith [2] in the Middle Jurassic deep-water shaly matrix, thus forming a Jurassic olistostroma [30]. Triassic age of the reddish radiolarites was first determined by [68] at the Držkovce and Bohúňovo localities and later confirmed here by [69]. The Middle to early Late Jurassic (Bajocian to Oxfordian) radiolarians in pelagic shales were documented by [4]. Basic geochemical (whole-rock) data from the basalts of chosen localities were published by [4,5,27].

Pelagic sedimentation continued until the early Late Jurassic [4] and was followed by S-ward subduction of the oceanic and adjoining continental crust. The Jurassic sediments, termed “flysch” [4,8]), may contain Triassic olistoliths forming Jurassic olistostromes. These were reported from the Meliata

Unit s.s. in the Meliata and Jaklovce village areas [2,4,64], but the sediments also contain the HP to MP metamorphosed blocks of the Triassic successions at the Dobšiná and Jaklovce localities [8,70–73].

The Meliatic blocks and fragments of different (km–cm) size have major lithology and metamorphic overprinting grade differences and these currently remain subdivided into (i) a subducted part, metamorphosed at HP–MP/LT conditions and termed the Bôrka Nappe [8,29,30,74–76], and (ii) unsubducted fragments with only very low-grade metamorphic overprinting, termed the Meliata Unit s.s. according to the type locality at the Meliata village [1,2,4,8,30,64,76,77].

The Bôrka Nappe blueschist facies metabasalts associated with Rožňava Zone Triassic marbles exhibit intra-plate affinity [5,29], and continental arc basalts were also reported here by these authors. This situation imposes the Bôrka Nappe as a subducted Meliata Basin continental margin with deeper shelf to slope facies on the inferred Gemic-type basement. The estimated HP/LT metamorphic conditions are approximately 350–450 °C at 900–1200 MPa [29,78,79]. The timing of the ocean closure and subduction of the attenuated continental and inferred oceanic crust in the Late Jurassic is constrained to 160–150 Ma by  $^{40}\text{Ar}$ – $^{39}\text{Ar}$  [80–84] and K–Ar 155–152 Ma ages [84] of “phengitic” white micas from blueschists.

The Meliata Unit s.s. (defined at the Meliata village by [2]) is a Middle Jurassic deep-water turbiditic succession interlayered with radiolarites [85]. It contains fragments of the Triassic continental margin carbonates and rare inferred oceanic crust radiolarites [85]. Basalts are also uncommon there because only one fragment has currently been identified [64]). The whole unit has weak metamorphic overprinting at 257–312 °C/350–540 MPa and relatively younger metamorphic ages than the Bôrka Nappe at 150–115 Ma [40,80–84]. The Jurassic olistostromes of the Meliata Unit s.s. were drilled in borehole BRU-1 in the core of the “Brusník Anticline” in the southern part of the Slovenské Rudohorie Mts. [63], and this borehole confirmed tectonic position of the Turňa Nappe on the Meliata Unit s.s. The tectonic basement of the Meliata Unit s.s. was most likely formed by the Middle to Upper Triassic pale marbles of Honce-type limestones and some schistose limestones with basalts and basaltic tuff layers of the Dúbrava or Hačava formations [86] incorporated into the Bôrka Nappe. The high-T anchi-zone at 200–350 °C and 200–350 MPa was reported from the overlying Torna/Turňa Nappe [87].

Amphibole gabbros to dolerites and serpentinites are embedded in the Silicic Nappe Permian salinar formation near Gemerská Hôrka and Bohúňovo villages and similar fragments have also been identified in the Perkupa Formation in northern Hungary at the sole of the Silica Nappe [34]. In addition, Meliatic type deep-water Triassic successions occur in Permian evaporitic mélange at the base of the higher Mesozoic nappes of the Northern Calcareous Alps in Austria [3,41,42].

The very low-temperature thermo-chronological data at <180 °C from the Meliaticum [8] constrained the final exhumation and cooling history of the Meliatic accretionary wedge fragments to approximately 130–100 Ma by zircon (U–Th)/He (ZHe) dating. The youngest ZHe ages of 80–65 Ma obtained from the Meliatic Jaklovce fragment and the underlying Gemicum are post-thrust- or post-nappe-formation ages. These ages conform to the post-collisional zircon fission track (ZFT) ages of 88 to 62 Ma from the Gemic and Veporic tectonic units [88,89]. The oldest apatite (U–Th)/He (AHe) age of ca. 63 Ma obtained from rodingite at Dobšiná may indicate cooling of the Meliatic fragments within the IWC orogenic wedge below approximately 70 °C [8]. This age is consistent with the apatite FT ages of 63–55 Ma and AHe ages of 62–31 Ma from the southern Veporicum [89].

Serpentinized ultramafic bodies of the Meliaticum were reported by [26]. Their genetic aspects were published by [7,90–92], who assigned them to the abyssal peridotites.

The HP mélange blocks are embedded in serpentinitic sandy matrix and finally tectonically mixed with the unmetamorphosed to anchimetamorphosed Jurassic flysch sediments at Dobšiná [8]. The 135 Ma U–Pb SIMS [92] and LA–ICP–MS [73] age of metamorphic–metasomatic Prv ( $\epsilon\text{Nd}_{135} = -8$ ) in serpentinitized abyssal harzburgites [93,94] and rodingites and the whole-rock and mineral trace element study [90] constrain the interaction of these ultramafics with the Meliatic accretionary wedge fluids.

While our review of published results documents that geologists previously concentrated on the Meliata Unit s.s. and the Bôrka Nappe, herein we continue our research around Dobšiná town

and Jaklovce village because these provide new information on the complicated *mélange* structure. We focused on the *mélange* blocks' rock composition to reconstruct the main Meliatic paleotectonic zones from the *mélange* sources, with the respect to geochemical, biochronological, and geochronological constraints. We also performed comparative studies with other Meliatic localities, including Malý Radzim at Brdárka, Meliata, Bretka, Čoltovo, Hačava, and Šugov Valley, with emphasis on inferred oceanic crust fragments which are typical neither for the Meliata Unit s.s. nor the Bôrka Unit, but typical of the newly-defined Jaklovce Unit. The types of the *mélange* matrix and the metamorphic overprinting signatures of both the *mélange* blocks and the Jurassic sedimentary matrix are then addressed and the obtained dataset was used to outline a tentative evolutionary model of Meliaticum.

### 3. Research Methods

This paper summarizes results from detailed field studies of the chosen lithological cross-sections performed to determine the *mélange* rock-composition, whole-rock chemical compositions including REE and Nd isotopic determinations, and also to assess the Zrn and Rt isotopic age data from the Meliatic *mélange* blocks.

The field investigation was focused on lithologically variable inferred continental margin and/or oceanic Middle Triassic to Lower Jurassic fragments associated with the Jurassic flysch sediments in the *mélange*. The mineral composition and textures of the studied basalts and related sedimentary rocks were investigated in polished sections by polarized light microscope. The mineral element compositions were measured by electron probe microanalysis (EPMA) on a Cameca SX-100 electron microprobe at the State Geological Institute of Dionýz Štúr in Bratislava, and by JEOL Super-probe JXA 8100 at the Earth Science Institute of Slovak Academy of Sciences in Banská Bystrica (Slovakia). The petrographic rock description is based on our previously published mineral chemical composition and classification data [7,72], further literature data [29,79], and our new, so far unpublished data available in Supplementary Figures S1–S4 and Tables S1 and S2.

The pulp samples were analyzed by X-ray fluorescence (XRF) for major elements, and the trace and rare earth elements (REE) were determined in ACME Laboratories Ltd. in Vancouver, BC, Canada. Instruments for inductively coupled plasma optical emission spectrometry (ICP-OES) and inductively coupled plasma mass spectrometry (ICP-MS) were used for whole-rock (including REE) geochemical analyses ([acmelab.com/services/general-conditions-of-service/](http://acmelab.com/services/general-conditions-of-service/)).

The Zrn and Rt crystal samples were mounted in a transparent epoxy and polished to expose the interior of the crystals, and mounts were coated with high-purity gold to reach  $<20 \Omega$  resistance prior to analysis. High-quality images of Zrn and Rt crystals under translucent and reflective light and Scanning Electron Microscope Cathodoluminescence (SEM-CL) images were available for spot choice to avoid fractures and inclusions. Measurements of U, Th, and Pb isotopes in Zrn and Rt were made by Cameca IMS-1280HR SIMS at the Institute of Geology and Geophysics, Chinese Academy of Sciences in Beijing, China. The complete instrument description and analytical procedure for zircon are described in [95], for rutile in [96].

The primary beam of  $O_2^-$  was accelerated at 13 kV and focused to an ellipsoidal spot of approximately 20 by 30  $\mu m$  in size. Positive secondary ions were extracted with a 10kV potential. A mass resolution of approximately 5400 defined at 10% peak height separated  $Pb^+$  peaks from isobaric interference. A single electron multiplier in ion-counting mode measured secondary ion beam intensities by peak jumping mode. For zircon, Pb/U calibration was performed relative to the Plešovice Zrn standard ( $^{206}Pb/^{238}U$  age = 337 Ma, [97]), and U and Th concentrations were calibrated against Zrn standard 91500 (Th = 29 ppm, and U = 81 ppm, [98]). The Qinghu Zrn standard was alternately analyzed as one of the unknowns in order to monitor the external uncertainties. Twenty-two Qinghu Zrn measurements yielded a Concordia age of  $160 \pm 1$  Ma, and this is identical within error with the recommended value of  $159.5 \pm 0.2$  Ma [99]. For rutile, U-Pb ratios and absolute abundances were determined relative to rutile standard DXK [96]. A regression line on the Tera-Wasserburg Plot with total Pb ratios was constructed to calculate the lower intercept as the rutile age. In addition, the

analytical uncertainties for the single spot were listed in 1 sigma level, and the quoted Concordia U–Pb ages are within the 95% confidence interval. All Concordia age diagrams were generated by Isoplot/Ex program (Version 2.49, Berkley Geochronology Center, Berkeley, CA, USA) [100].

The whole-rock Sm–Nd isotopic ratios were measured by thermal ionization mass spectrometry (TIMS) at the State Key Laboratory of Continental Dynamics, Northwest University, Xi’an, China, and the complete analytical procedure is described in [101]. The Nd isotopic mass fractionation was corrected by the natural  $^{146}\text{Nd}/^{144}\text{Nd}$  ratios of 0.7219, and the age-corrected  $^{147}\text{Sm}/^{144}\text{Nd}$  ratios were calculated using the Sm and Nd concentrations obtained by ICP–MS in ACME Laboratories Ltd. in Vancouver, BC, Canada.

The choice of cherty rock samples for biostratigraphic research was based on the examination of thin sections to avoid strongly deformed and recrystallized domains and to find the radiolarian-bearing layers. The metamorphic alteration of these rocks made it very difficult to extract radiolarians despite avoiding metamorphic veins and veins cross-cutting metacherts. Fifteen samples of cherts and cherty shales were processed to extract radiolarians with the rocks broken to a few centimeter size and soaked in hydrochloric acid. The remaining samples were dissolved in diluted (3%) hydrofluoric acid, and the radiolarians were extracted from the residues and studied by Scanning Electron Microscope (SEM) for more precise determination. Approximately 180 radiolarian specimens from the Jaklovce samples were studied and their pictures were recorded by SEM.

## 4. Results—Mélange Block Description

### 4.1. Mélange Rock-Composition

Two contrasting mélangé kilometer-size blocks overlie the Upper Carboniferous or Permian–Lower Triassic cover of the Gemicum in the Dobšiná town area (Figure 3).

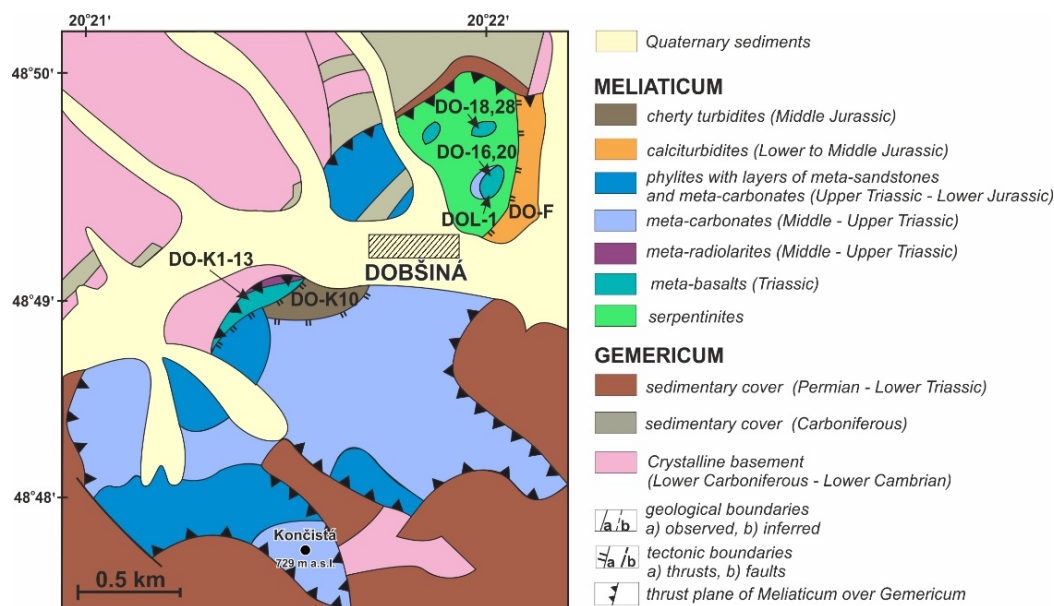
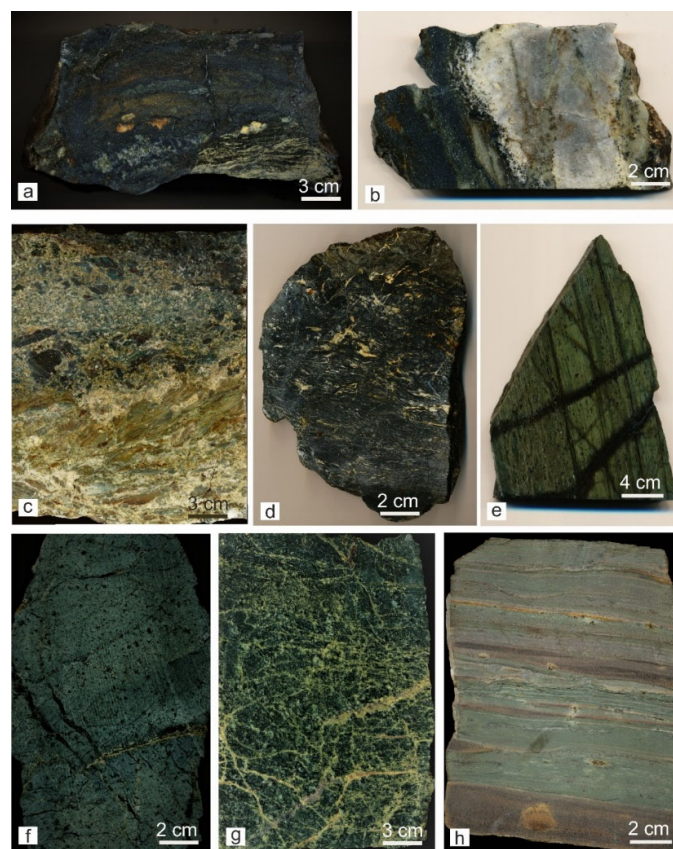


Figure 3. Schematic geological map from Dobšiná area (modified from [44]) with sample location.

Figures 3 and 4 highlight a mélangé block composed of lensoidal to almost spherical fragments of serpentinitized peridotites, rodingites, blueschists, marbles, and Tlc–Chl–Phg–Cal schists flowing in the soft serpentinitic sandy matrix exposed in a quarry north of Dobšiná town. Part of the blueschist lenses is present in the hosting metasediments, and their contacts are barely recognizable (Figure 5a–c). However, most of the basalt and peridotite bodies are directly in the serpentinitic matrix and many have mylonitic to cataclastic deformations (Figure 5d,e). This large serpentinitic mélangé block is in tectonic contact with overlying Jurassic calciturbidite deposits (Figure 4).



**Figure 4.** The Dobšiná quarry serpentinitic mélange block with a 4 m long blueschist lens in contact with marble and Tlc-Chl-Phg-Cal schist fragments and Jurassic calciturbidite deposits.



**Figure 5.** Rock fragments from serpentinitic mélange matrix in contact with marly shales N of Dobšiná (a)–(e): (a) Blueschist layer (dated sample DOL-1) in Tlc-Phg-Chl-Cal schist (lower right-hand corner). (b) Blueschist layer in marble. (c) Tectonized contact of a blueschist (top) and Tlc-Phg-Chl-Cal schist with pale calcite mobilizates. (d) Blueschist mylonite. (e) Serpentinized harzburgite mylonite. Metabasalt layers in metaradiolarites S of Dobšiná (f)–(g). (f) Metabasalt (sample DO-K12). (g) Metadolerite (sample DO-K13). (h) Jurassic calciturbidites (sample DO-F) composed of calcareous shales with millimetric to centimetric greenish clayey-marly and brownish carbonate-rich sandy layers (a quarry N of Dobšiná).

The second type mélange block occurs S of Dobšiná in the Končistá Hill area. It consists of laminated cherty shales to radiolarites associated with basalts to dolerites (Figure 3, Figure 5f,g).

Further to the S of Dobšiná, below the Malý Radzim Silica Nappe outlier (near Brdárka locality), the blueschists (sample MR-1) associate with rare cherts (Figure 2). The Permian siliciclastics, rhyolitic volcanoclastics, and mid-Triassic marbles in their vicinity are assigned to the Bôrka Nappe [8].

The Jurassic calciclastic deposits (calciturbidites~calcareous flysch) at Dobšiná (Figure 3, Figure 4, Figure 5h) consist of calcareous shaly layers interbedded with carbonatic sandstones. The calciturbidite beds are laminated and contain an admixture of Qz, Ms, Pl/Ab, and rare Tur in sandstone layers.

We then investigated a large mélangé block in the Jaklovce village area which has cherty sediments alternating with basalts in tectonic contact with calciturbidites (calcareous flysch), as in Dobšiná (Figure 6). The studied cross-section begins in a railway-cutting north of the Jaklovce village at the Calmit company. This then continues through the village along a main road-cutting to Gelnica to the west or to a forest road-cutting above the main road to the Veľký Folkmár village to the S. Sedimentary bedding and parallel metamorphic schistosity are approximately S-dipping at a medium angle in the exposed northern part of the cross-section depicted in Figure 6.

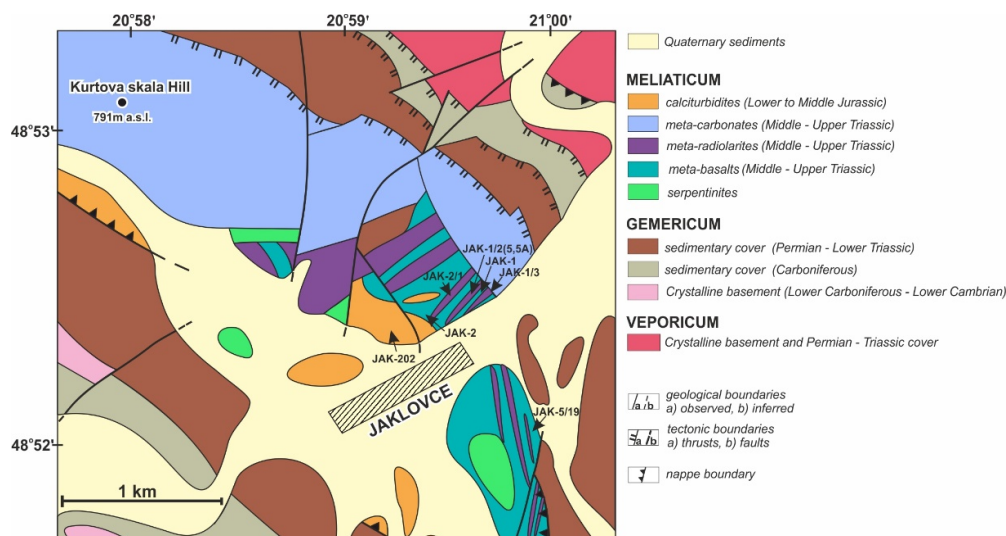
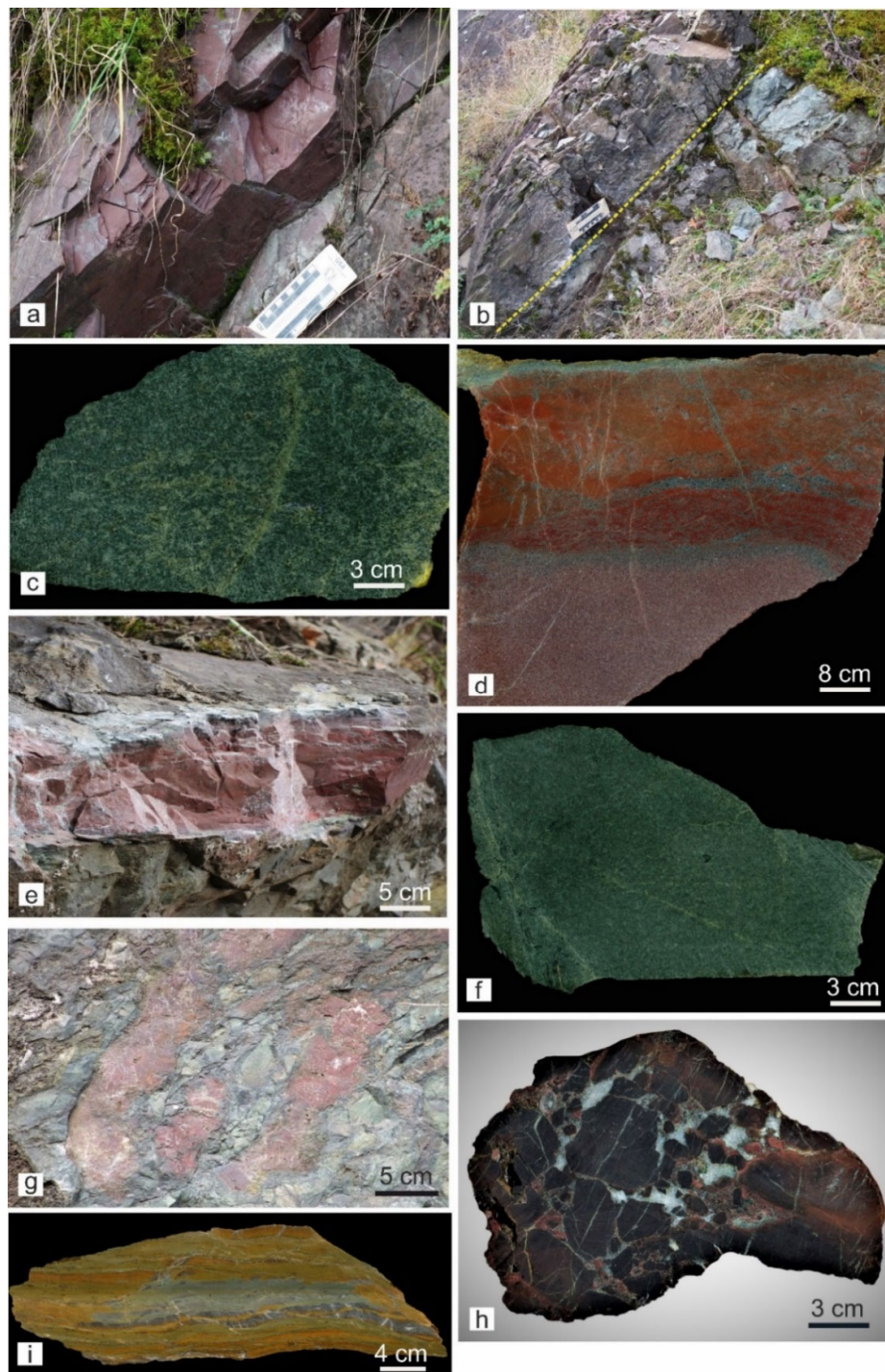


Figure 6. Schematic geological map from Jaklovce area (modified from [44]) with sample location.

Our Figure 7a highlights that this cross-section begins with reddish cherty shales with thin cherty carbonate laminae, followed upwardly by a few-meter-thick greenish to reddish schistose cherty shales to massive radiolarites (Figure 7b) with a half-meter thick basalt layer (Figure 7b,c). Pelagic reddish carbonates form a few-decimeter-layer in the western part of the cross-section, and this passes upwardly into cherty carbonates, dark-red cherty clayey-carbonatic shales, and pale-red radiolarites with basaltic tuff layers (Figure 7d). Regularly alternating radiolarites and basalts (Figure 7e,f) are often disturbed by peperitic breccia horizons (Figure 7g) which formed from the interaction of quickly quenching basaltic lava flows and unlithified water-soaked reddish clayey, cherty, and radiolarite sediments. Finally, basaltic lava flow breccias (Figure 7h) interlayered with reddish radiolarites were identified south of the Jaklovce village center above the main road to Veľký Folkmár village.

Serpentinities are an integral part of the mélangé, and the largest lens is sandwiched between the top Triassic carbonatic succession of the Kurtova skala Hill and the bottom Jurassic calcareous flysch N of Jaklovce (Figure 6). The rigid, partly detached carbonatic sheet of the Kurtova skala Hill overthrusts the Gemic Permian volcano-sedimentary and the Lower Triassic siliciclastic cover.



**Figure 7.** Rock lithology from the oceanic Jaklovce Succession. (a) Reddish cherty schists from the Lower Beds with Ladinian radiolarians (s. JAK-1/3). (b) Alternation of reddish and greenish cherty schists (s. JAK-1/2–JAK-5, 5A) to metaradiolarites with a half-meter thick metabasalt layer (s. JAK-1, below dashed line) from the Middle Beds. (c) Detailed view on metabasalt s. JAK-1. (d) Reddish carbonate (bottom) passing upwards into the middle dark-red cherty clayey-carbonatic shale (s. JAK-2/1 with Middle to Upper Triassic radiolarians) and the top radiolarite with basaltic tuff layer. (e) Regular alternation of metabasalts (f) and metaradiolarite layers is often disturbed by (g) Peperitic breccias. (h) Brecciated margin of a lava flow with secondary Cal infilling cracks (s. JAK-5/19). (d)–(h) The Upper Beds. (i) Jurassic calciturbidites (calcareous flysch) with brownish carbonatic sandstone layers (s. JAK-202).

The investigated blocks are tectonically mixed with the Jurassic calcareous flysch formation (Figure 7i) and small metric-size sedimentary matrix exposures are rarely present among the rigid mélangé blocks (Figure 6). Although the calcareous flysch sediments lithologically and petrographically closely resemble the Dobšiná marlstones featured in Figure 5, this Jurassic sediment type is different to the dark clayey to cherty shales (siliciclastic flysch) with radiolarites described at the Meliata village [2–4,85].

#### 4.2. Biochronology

The Jaklovce mélangé block reddish and greenish cherty shales contain siliceous microfauna. The eastern part of the investigated cross-section begins with reddish cherty shales (sample JAK 1/3, Figure 7a) in the Lower Beds of the oceanic Jaklovce Succession. Their radiolarian microfauna is dominated by large-sized spherical spumellarians such as *Archaeocenosphaera* sp., *Cenosphaera* sp., *Entactinia* sp., and additional indeterminate genera and species. In addition to the simple spumellarians, there are also spine-bearing tests from the following species; *Pseudostylosphaera japonica*, *Pseudostylosphaera* cf. *coccostyla*, *Pseudostylosphaera compacta*, *Capnuchosphaera* cf. *triassica*, *Monostylosphaera* sp., *Muelleritortis* cf. *cochleata*, *Muelleritortis firma*, *Tiborella* cf. *anisica*, and *Parasepsagon* cf. *variabilis* (Figure 8, images 1–9). This association indicates a Middle Triassic age of the radiolarites from the Lower Beds of the Jaklovce Succession, and the numerous radiolarians of *Muelleritortis* and *Pseudostylosphaera* species imply Ladinian zones (cf. [102–105]).

The Middle Beds of the oceanic Jaklovce Succession are formed by greenish and reddish cherty shales (s. JAK-1/2, Figure 7b). These beds contain the first (N-MOR) basalt extrusion layer which is approximately 0.5 m thick. Here we found slightly younger late Ladinian to Carnian microfauna with increased nassellarian-type radiolarians. Their association comprises species *Corum kraineri*, *Triassocampe scalaris*, *Annulotriassocampe* sp., *Japonocampe* sp., *Eppingium* cf. *manfredi*, *Pseudostylosphaera* cf. *tenuis*, and *Spongoxystris* cf. *slovenica* (Figure 8, images 10–18).

The Upper Beds of the oceanic Jaklovce Succession have polygenic lithologies of red cherts alternating with (N-MOR) basalts. Cherty clayey-carbonatic shale (sample JAK-2/1; Figure 7c, the middle dark-red layer) contains poorly preserved radiolarians (Figure 8, images 19–23). Although precise determination is difficult, there is a predominance of spherical spumellarians such as *Archaeocenosphaera* sp., *Capnuchosphaera* sp., and *Entactinia* sp. The scarce nassellarian-type radiolarians include tiny conical forms of *Triassocampe* sp., *Annulotriassocampe* sp., and *Whalenella* sp. This association differs from radiolarians of the Lower and Middle Beds through their lack of Ladinian *Muelleritortis* and *Pseudostylosphaera* sp. and the inclusion of younger *Capnuchosphaeridae* and *Triassocampidae* sp. This is also differentiated by pantanellids which appeared in the late Carnian [106], and therefore the late Carnian (Late Triassic) age for the Upper Beds of the oceanic Jaklovce Succession is constrained.

The Jurassic calciclastic sequence at Dobšiná contains fine-grained sandstone layers with dishlike structures resembling the internal moulds of *Posidonia*-type bivalves. These fossils may constrain late Early to Middle Jurassic age for this trench-like calcareous flysch succession (Toarcian–Bathonian). In addition, radiolarians in the dark cherty shales from the Meliata locality establish that the entire Jurassic succession terminated in the early Oxfordian [85].

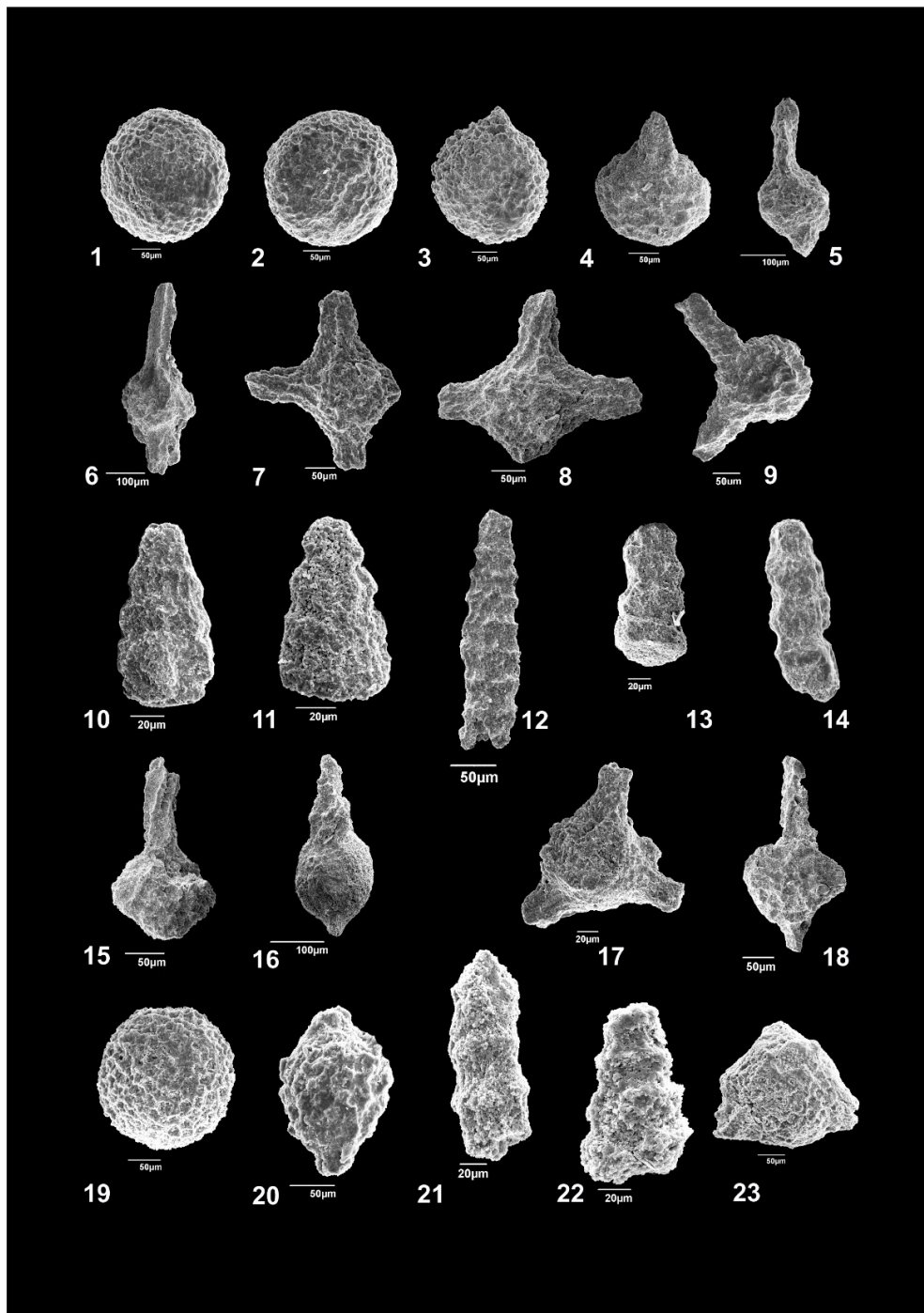


**Figure 8.** Triassic radiolarian microfauna from the Jaklovce cross-section. Images 1–9 Ladinian radiolarians from cherty shales and radiolarites of the Lower Beds (s. JAK 1/3): 1, 2—*Archaeocenosphaera* sp.; 3, 4—*Spumellaria* gen. et sp. indet.; 5—*Pseudostylosphaera nazarovi*; 6—*Pseudostylosphaera japonica*; 7—*Muelleritortis firma*; 8—*Muelleritortis cf. cochleata*; and 9—*Capnuchosphaera? triassica*. Images 10–18 late Ladinian–early Carnian radiolarians from cherty shales of the Middle Beds (s. JAK 1/2): 10, 11—*Corum kraineri*; 12—*Triassocampe scalaris*; 13—*Triassocampe cf. scalaris*; 14—*Annulotriassocampe* sp.; 15—*Spongoxystriis cf. slovenica*; 16—*Spongoxystriis* sp.; 17—*Eppingium cf. manfredi*; and 18—*Pseudostylosphaera cf. tenuis*. Images 19–23 middle to late Carnian radiolarians from dark-red cherty clayey carbonatic shale of the Upper Beds (s. JAK 2/1): 19—*Archaeocenosphaera* sp.; 20—*Pantanellium* sp.; 21—*Annulotriassocampe* sp.; 22—*Triassocampe* sp.; and 23—*Capnuchosphaera* sp.

### 4.3. Petrography and Geochemistry

#### 4.3.1. Dobšiná Area Metabasalts

A mélange block north of Dobšiná town contains Gln-bearing blueschist fragments (Figure 5a–d, Figure 9a,b, Figures S1 and S2; Table S1). The Gln overgrowing Mg-Rbk form part of the peak HP metamorphic assemblage with Tlc, Chl, Phg, Ep, and Jd relics in Ab. A mélange block south of this town contains the MP greenschist-facies metabasalt with Act, Chl, Phg, Ep, Cal, Ttn, and Ab comprising the mineral assemblage (Figure 9c,d, Figures S1 and S2; Table S1). Figure 2 herein depicts a blueschist-facies metabasalt fragment (Figure 9e,f) further south and below the Malý Radzim Hill at Brdárka. Finally, Table 1 identifies the whole-rock geochemical compositions of these metabasalts and Table 2 reveals the Nd isotopic data from different original basalt types.

The blueschist-facies metabasalt of the DOL-1 sample, analogous with DO-16 and 20 samples, has interlayers of Lower/Middle Triassic carbonate-marly sediments incorporated in a mélange block serpentinitic sandy matrix (Figure 3, Figure 4, Figure 5a). These have the highest content of SiO<sub>2</sub>, Al<sub>2</sub>O<sub>3</sub> and the Na<sub>2</sub>O, and K<sub>2</sub>O alkalis and lowest TiO<sub>2</sub> and CaO of all investigated metabasalts. In addition, they have abundant Rb, Ba, Ce and La, LILE and also U, Th, and Be, with characteristic negative Eu anomaly and negative  $\epsilon\text{Nd}_{250} = -6.41$  value (DO-16 sample). This group of metabasalts is characterized by transitional sub-alkaline to alkaline nature with  $\sim 0.7$  Nb/Y ratio, relatively low 0.02 Zr/TiO<sub>2</sub> (Figure 10 [107]) and also low 0.80 to 0.89 TiO<sub>2</sub> content and generally high 138–151 ppm Zr. The distribution of other incompatible elements and their concentrations and ratios such as Co (25–26 ppm), Nb/Yb ( $\sim 6.3$ ), Ta/Yb (0.44–0.52), and Th/Yb ( $\sim 4.5$ ) indicate that these rocks share affinity with calc-alkaline volcanic arc basalts or slab-distal (fore)back-arc basin basalts (Figures 11–14 [108–111]). The chondrite-normalized REE abundances in this group of volcanic rocks have regularly decreasing patterns from LREE to HREE with (La/Yb)<sub>N</sub> ratios ranging from 9.8 to 10.9. Finally, the La generally varies from  $\sim 158$  to  $\sim 168$  times the chondrite abundance and 53 to 59 times the primitive mantle abundance (Figure 15; cf. Figure S3 with rock/primitive mantle normalization), and the rock's REE patterns are consistent with calc-alkaline affinity [112–115].

Samples DO-18 and 28 provide a further blueschist-facies metabasalt lens in the same large mélange block north of Dobšiná (Figures 3 and 4). These have medium SiO<sub>2</sub>, CaO, and K<sub>2</sub>O content compared to the former group with the highest TiO<sub>2</sub>, the lowest MgO and increased Na<sub>2</sub>O. They also have abundant HFSEs (Zr, Hf, Nb, Ta), Eu, Sm, Nd, with  $\epsilon\text{Nd}_{240} = 4.89$  in the DO-18 sample. This second group exhibits alkaline nature with high Nb/Y ratios ( $\sim 1.0$ – $1.2$ ) and low Zr/TiO<sub>2</sub> ( $\sim 0.01$ ) (Figure 10 [107]). These metabasalts are also characterized by very high 2.96–3.00 wt. % TiO<sub>2</sub> content, 147–164 Ti/V ratios and high 209–218 ppm Zr. Other incompatible element contents and ratios include Co (13.7–21.9 ppm), Nb/Yb (11.9–13.47), Ta/Yb (0.76–0.78), and Th/Yb (0.79–0.81). These are comparable to typical intra-plate alkaline basalts, such as ocean island basalts (OIB). The discrimination diagrams in Figures 11–14 [108–111] highlight that these rocks plot in the fields for alkaline oceanic within-plate basalts (WPB) and in oceanic subduction-unrelated settings, and they display significant LREE enrichment over HREE (Figure 15; cf. Figure S3 with rock/primitive mantle normalization). This is exemplified in their 5.4–6.2 (La/Yb)<sub>N</sub> ratios and the overall REE enrichment ranges from  $\sim 20$  to  $\sim 120$  Yb times the chondrite abundance and from  $\sim 6$  to  $\sim 40$  La times the primitive mantle abundance [112].

**Table 1.** Major and trace elements from the whole-rock XRF and inductively coupled plasma mass spectrometry (ICP–MS) analyses. LOI = Loss on ignition.

Locality	Dobšiná				Radzim				Jaklovce						V.Folkmár		Bretka	Šugov	Meliata	Čoltovo	Hačava	
Sample	DO-16	DO-20	DO-18	DO-28	DO-K1	MR-1	JAK-1	JAK-2	JAK-2A	JAK-3	JAK-4	JAK-6A	JAK-6B	JAK-18	JAK-22	VFK-1	BRT-1A	SUG-10	MEL-15	COL-1	HAC-1	
wt. %																						
SiO <sub>2</sub>	59.54	59.96	51.39	53.03	49.47	47.21	39.63	46.90	47.80	49.82	48.55	48.05	48.63	43.37	47.63	46.47	49.51	54.63	43.79	45.78	49.55	
TiO <sub>2</sub>	0.89	0.80	2.96	3.00	0.15	1.71	1.72	1.92	1.97	1.96	1.55	1.52	1.55	2.95	2.67	1.97	1.44	2.40	1.62	0.79	2.92	
Al <sub>2</sub> O <sub>3</sub>	16.89	16.81	16.13	15.58	14.44	14.88	12.13	16.11	13.65	13.72	14.58	14.79	14.69	14.56	14.02	13.53	15.14	13.12	14.22	14.27	13.02	
Fe <sub>2</sub> O <sub>3</sub> T	4.57	5.42	13.20	12.24	10.42	14.08	12.98	9.36	12.21	12.07	9.99	10.29	8.92	16.59	15.08	11.08	12.22	14.27	7.63	7.77	15.28	
MgO	9.40	7.49	3.94	3.17	8.14	9.20	6.86	7.01	6.55	6.88	7.55	7.77	7.23	7.58	6.25	8.18	6.41	1.97	3.86	4.04	4.30	
CaO	0.85	0.69	4.18	5.01	6.97	3.46	17.31	8.49	9.92	8.82	10.54	10.36	11.63	6.34	6.58	6.68	6.85	5.06	11.92	10.40	3.75	
Na <sub>2</sub> O	6.63	7.72	6.14	6.55	4.33	3.89	1.64	4.53	3.90	3.87	3.61	3.42	3.60	3.62	3.69	4.05	4.80	4.53	4.82	5.63	3.45	
K <sub>2</sub> O	2.18	1.08	0.52	0.57	1.66	1.40	0.06	0.13	0.23	0.39	0.19	0.16	0.06	0.11	0.05	1.71	0.18	1.40	0.03	0.11	4.09	
P <sub>2</sub> O <sub>5</sub>	0.14	0.12	0.13	0.68	0.15	0.14		0.20	0.20	0.20	0.15	0.15	0.15	0.31	0.28		0.14	0.85	0.16	0.11	0.70	
MnO						0.13	0.23	0.29	0.19	0.18	0.17	0.18	0.17	0.19	0.09			0.13	0.24	0.16	0.18	
Cr <sub>2</sub> O <sub>3</sub>						0.03	0.36	0.05	0.02	0.02	0.04	0.04	0.04	0.01	0.01				0.03	0.05		
LOI			1.60		4.10	3.60	7.00	4.70	3.20	1.80	2.90	3.00	3.10	4.10	3.30	6.10	3.10	1.40	11.50	10.70	2.40	
Total	101.10	100.08	100.20	99.83	99.83	99.73	99.92	99.69	99.84	99.73	99.82	99.73	99.77	99.73	99.65	99.77	99.79	99.76	99.82	99.81	99.64	
ppm																						
Sc	20.00	19.00	17.76	19.97	40.00	41.00	38.00	41.00	45.00	44.00	41.00	41.00	41.00	53.00	48.00	37.00	41.00	30.00	36.00	26.00	34.00	
V	125	116	181	204	310	294	381	340	380	390	320	319	321	540	490	313	285	140.00	282	145	285	
As	2.30	2.65	9.76	8.90	1.80	2.40	11.50	3.80	18.60	17.10	3.60	5.20	4.90	20.40	27.00	4.10	5.60	8.70	1.60		13.30	
Rb	94	57.46	12.38	12.41	2.80	49.40	1.90	3.80	5.00	9.80	4.30	3.70	0.80	3.70	2.00	57.30	1.50	52.10	0.90	3.10	111	
Sr	16.80	18.25	100	109	101	156	390	228	153	138	194	208	213	111	126	247	133	111	161	91	61.90	
Y	22.88	23.21	37.21	34.72	31.70	29.20	41.90	34.80	38.50	38.30	30.50	31.00	31.00	53.80	51.90	27.20	24.80	84.90	26.40	13.20	79.20	
Zr	151	139	209	218	108	115	105	123	113	140	88.10	93.30	86.90	172	165	119	84.70	385	113	39.90	348	
Nb	16.65	16.27	35.84	42.56	4.30	2.00	2.90	3.40	3.40	3.40	2.10	2.30	2.20	5.60	5.60	3.70	4.50	14.90	4.10	1.90	14.40	
Cs	12.30	14.55	0.47	0.45	0.10	1.60	0.30	0.30	0.60	1.90	0.40	0.50	1.30	3.20	2.80	1.80	0.10	3.40	0.40	0.30	4.70	
Ba	210	154	88	105	11.00	117	9.00	19.00	18.00	29.00	23.00	27.00	33.00	17.00	13.00	129	23.00	178	13.00	15.00	591	
Hf	4.14	3.88	5.22	5.88	3.20	3.00	2.80	3.20	3.20	3.80	2.60	2.70	2.70	4.60	4.40	3.33	2.40	10.10	3.00	1.20	8.70	
Ta	1.15	1.35	2.29	2.46	0.90	0.10	0.20	0.20	0.20	0.20	0.20	0.20	0.20	0.50	0.40	0.20	0.30	1.30	0.20	0.09	1.00	
Pb	1.70	0.80	2.10	1.85	1.20	3.10	2.80	1.70	6.20	1.30	0.60	1.50	3.80	1.30	1.30	1.10	1.60	1.50	0.70	0.70	2.30	
Be	2.79	3.01	1.08	1.60	0.90	0.90	2.00	0.90	0.90	0.90	0.90	0.90	0.90	0.90	0.90	0.90	0.90	2.00	0.90	0.90	6.00	
La	42.07	37.49	23.79	28.91	3.70	4.00	4.70	5.80	4.50	4.30	3.10	3.40	3.20	8.10	8.90	4.90	6.60	33.90	6.70	5.90	33.30	
Ce	93.76	96.47	56.83	64.01	10.40	11.30	13.50	15.50	13.70	13.30	10.00	10.30	9.90	22.50	21.70	11.00	13.20	79.30	21.50	11.10	73.40	
Pr	8.91	9.48	7.37	8.65	1.68	1.89	2.21	2.52	2.31	2.29	1.73	1.75	1.73	3.67	3.81	1.63	2.20	10.64	3.00	1.47	9.99	
Nd	31.90	35.43	33.12	38.63	9.00	9.90	11.50	12.60	13.20	12.30	9.60	10.40	10.20	20.70	20.40	8.30	11.50	47.50	14.10	6.30	45.00	
Sm	5.68	6.34	8.04	9.03	3.20	3.27	4.23	3.92	3.50	3.53	2.81	2.82	2.80	5.48	5.25	2.90	3.39	12.92	3.69	2.03	12.13	
Eu	0.86	0.83	2.54	2.95	1.17	1.13	1.46	1.42	1.38	1.35	1.11	1.15	1.08	1.95	1.86	1.11	0.92	3.53	0.98	0.86	3.47	
Gd	4.75	5.10	8.32	8.98	4.55	4.20	5.86	5.62	5.42	5.45	4.25	4.39	4.32	8.05	7.81	4.20	4.05	14.88	4.59	2.62	14.68	
Tb	0.70	0.75	1.25	1.36	0.86	0.82	1.05	0.96	0.90	0.90	0.72	0.73	0.72	1.33	1.26	0.75	0.72	2.63	0.75	0.43	2.37	
Dy	4.03	4.25	7.07	7.59	5.63	5.41	7.00	6.19	6.34	6.67	5.14	5.32	5.13	9.37	8.85	5.00	4.59	15.62	4.66	2.89	14.76	
Ho	0.84	0.88	1.36	1.47	1.19	1.16	1.50	1.31	1.39	1.46	1.17	1.12	1.13	2.02	1.90	1.08	1.01	3.45	0.99	0.58	3.11	
Er	2.48	2.54	3.53	3.77	3.76	3.39	4.45	3.73	4.12	4.07	3.32	3.30	3.37	5.73	5.44	3.34	2.93	9.96	3.06	1.70	9.05	
Tm	0.39	0.39	0.49	0.51	0.52	0.52	0.64	0.54	0.53	0.54	0.41	0.43	0.43	0.75	0.68	0.50	0.44	1.41	0.44	0.23	1.29	
Yb	2.63	2.60	3.01	3.16	3.38	3.14	4.06	3.47	3.78	3.95	3.08	3.05	3.08	5.34	4.89	3.15	2.82	8.88	3.01	1.43	7.65	
Lu	0.40	0.39	0.43	0.45	0.49	0.51	0.64	0.53	0.58	0.60	0.47	0.46	0.47	0.81	0.72	0.49	0.45	1.36	0.45	0.22	1.16	
Th	11.88	11.71	2.44	2.51	0.50	0.20	0.30	0.30	0.20	0.30	0.20	0.20	0.20	0.40	0.50	0.50	0.70	7.50	0.20	0.10	6.60	
U	2.07	1.95	0.80	0.86	0.20	0.10	2.30	0.10	0.20	0.10	0.10	0.10	0.10	0.80	1.50	1.20	0.30	2.50	0.30	0.10	2.20	
Co	25.90	24.60	21.90	13.70	33.30	23.10	35.90	30.70	43.90	39.40	35.80	35.50	29.30	44.90	58.40	5.70	45.30	18.30	9.20	18.70	21.90	
Sm/Nd	0.18	0.18	0.24	0.23	0.36	0.33	0.37	0.31	0.27	0.29	0.29	0.27	0.27	0.26	0.26	0.35	0.29	0.27	0.26	0.32	0.27	
Zr/Hf	36.51	35.68	40.07	37.12	34.28	38.20	37.50	38.41	35.31	36.87	33.88	34.56	32.19	37.43	37.41	35.59	35.29	38.10	37.60	33.25	40.05	
Ba/Th	17.66	13.18	35.85	41.95	22.00	585	30.00	63.33	90.00	96.67	115	135	165	42.50	26.00	258	32.86	23.73	65.00	150.00	89.55	

Table 1. Cont.

Locality	Dobšiná					Radzim			Jaklovce						V.Folkmár	Bretka	Šugov	Meliata	Čoltovo	Hačava	
Sample	DO-16	DO-20	DO-18	DO-28	DO-K1	MR-1	JAK-1	JAK-2	JAK-2A	JAK-3	JAK-4	JAK-6A	JAK-6B	JAK-18	JAK-22	VFK-1	BRT-1A	SUG-10	MEL-15	COL-1	HAC-1
Nb/U	8.06	8.35	44.80	49.49	21.50	20.00	1.26	34.00	17.00	34.00	21.00	23.00	22.00	7.00	3.73	3.08	15.00	5.96	13.67	19.00	6.55
Ce/Pb	55.15	121	27.06	34.60	8.67	3.65	4.82	9.12	2.21	10.23	16.67	6.87	2.61	17.31	16.69	10.00	8.25	52.87	30.71	15.86	31.91
Nb/Ta	14.47	12.05	15.62	17.29	4.78	20.00	14.50	17.00	17.00	17.00	10.50	11.50	11.00	11.20	14.00	18.50	15.00	11.46	20.50	21.11	14.40
Th/U	5.75	6.00	3.05	2.91	2.50	2.00	0.13	3.00	1.00	3.00	2.00	2.00	2.00	0.50	0.33	0.42	2.33	3.00	0.67	1.00	3.00
Ba/Rb	2.24	2.69	7.07	8.47	3.93	2.37	4.74	5.00	3.60	2.96	5.35	7.30	41.25	4.59	6.50	2.25	15.33	3.42	14.44	4.84	5.31
Ba/Cs	17.07	10.61	188	233	110	73.13	30.00	63.33	30.00	15.26	57.50	54.00	25.38	5.31	4.64	71.67	230	52.35	32.50	50.00	126
Rb/Cs	7.60	3.95	26.58	27.49	28.00	30.88	6.33	12.67	8.33	5.16	10.75	7.40	0.62	1.16	0.71	31.83	15.00	15.32	2.25	10.33	23.68
Zr/Sm	26.62	21.86	26.01	24.19	34.28	35.05	24.82	31.35	32.29	39.69	31.35	33.09	31.04	31.42	31.35	40.86	24.99	29.78	30.57	19.66	28.72
Hf/Nd	0.13	0.11	0.16	0.15	0.36	0.30	0.24	0.25	0.24	0.31	0.27	0.26	0.26	0.22	0.22	0.40	0.21	0.21	0.21	0.19	0.19
Y/Yb	8.69	8.92	12.35	10.99	9.38	9.30	10.32	10.03	10.19	9.70	9.90	10.16	10.06	10.07	10.61	8.63	8.79	9.56	8.77	9.23	10.35
Ta/Yb	0.44	0.52	0.76	0.78	0.27	0.03	0.05	0.06	0.05	0.05	0.06	0.07	0.06	0.09	0.08	0.06	0.11	0.15	0.15	0.15	0.15
Nb/Yb	6.32	6.26	11.90	13.47	1.27	0.64	0.71	0.98	0.90	0.86	0.68	0.75	0.71	1.05	1.15	1.17	1.60	1.68	0.16	0.14	0.18
Th/Yb	4.51	4.50	0.81	0.79	0.15	0.06	0.07	0.09	0.05	0.08	0.06	0.07	0.06	0.07	0.10	0.16	0.25	0.84	0.07	0.00	0.86
Zr/TiO <sub>2</sub>	0.02	0.02	0.01	0.01	0.07	0.01	0.01	0.01	0.01	0.01	0.01	0.01	0.01	0.01	0.01	0.01	0.01	0.02	0.01	0.01	0.01
Nb/Y	0.73	0.70	0.96	1.23	0.14	0.07	0.07	0.10	0.09	0.09	0.07	0.07	0.07	0.10	0.11	0.14	0.18	0.18	0.16	0.14	0.18
Th/Ta	10.32	8.67	1.06	1.02	0.56	2.00	1.50	1.50	1.00	1.50	1.00	1.00	1.00	0.80	1.25	2.50	2.33	5.77	1.00	1.11	6.60
Ti/V	71.52	68.97	164	147.18	4.84	58.16	45.14	56.47	51.84	50.26	48.44	47.65	48.29	54.63	54.49	62.94	50.53	122.14	57.45	54.48	103

There are metabasalt to metadolerite interlayered cherty schists to radiolarites in a mélangé block south of Dobšiná, and this is in tectonic contact with Jurassic flysch sediments (Figure 3). These metabasalts preserve the magmatic ophitic texture with pseudomorphs after Cpx, Amp, and lath-shaped Pl, the latter minerals partly to totally replaced by newly-formed Act, Ep, and Ab from the MP greenschist facies metamorphic overprinting (Figure 5f,g, Figure 9c,d).

Characteristic is the highest CaO, MgO, and Fe<sub>2</sub>O<sub>3</sub>T content, the lowest SiO<sub>2</sub> and alkalis (particularly K<sub>2</sub>O) and average TiO<sub>2</sub> compared to the alkaline and calc-alkaline basalts. While they are enriched in V and Sr, they are quite decreased in LILE and HFSEs. This group is represented by a sample DO-K1 which has low Nb/Y ratio of 0.14. They also have characteristically higher  $\epsilon\text{Nd}_{240} = 7.6$ , as in the DO-K4 basalt. The relatively high 0.07 Zr/TiO<sub>2</sub> was most likely increased by the Zrn xenocrysts in this sample (Figure 10 [107]), and it has very low 0.15 wt. % TiO<sub>2</sub> content and relatively low 110 ppm Zr and 31.7 ppm Y. Finally, the Ti/V ratio of 5 identifies the sample as boninite. However, due to the exceptionally low TiO<sub>2</sub> content. The discrimination diagrams in Figures 11–14 [108–111] highlight that this rock plots in the fields for basalts generated at mid-ocean ridge settings with a composition close to typical N-MORB. Figure 15 [116] shows that the sample's chondrite-normalized REE pattern is rather flat, and this is consistent with N-MORB compositions [113] because it exhibits LREE depletion  $(\text{La}/\text{Yb})_{\text{N}} = 0.74$  and overall HREE enrichment 21 times the chondrite abundance and of 7 times primitive mantle abundance.

Here, sample MR-1 is interesting because it highlights that only a Brdárka ophiolitic fragment south of Dobšiná and below the Radzim Hill Silicic Nappe outlier (Figure 2) is a true N-MORB-type blueschist ( $\epsilon\text{Nd}_{240} = 7.93$ , Tables 1 and 2). This sample has very low 0.07 Nb/Y and 0.01 Zr/TiO<sub>2</sub> ratios (Figure 10 [117]) which indicate its clear sub-alkaline nature. It has moderate 1.71 wt. % TiO<sub>2</sub> content and relatively low 110 ppm Zr and 29.2 ppm Y. In addition, the 58 Ti/V ratio and Nb(Ta)/Yb and Th/Yb values establish that this sample plots in the field for basalts generated at mid-ocean ridge settings (Figure 14 [111]) or along the MORB–OIB array towards relatively depleted compositions (Figure 12 [109]). In addition, Figure 15 shows that the chondrite-normalized REE pattern is very flat, and the  $(\text{La}/\text{Yb})_{\text{N}} = 0.9$  value is comparable to those with typical N-MORB composition. It has overall HREE enrichment 20 times chondrite abundance and of seven times primitive mantle abundance (Figure 15; cf. Figure S3). This basaltic rock plots in the typical N-MORB fields or in the boundary between N-MORB and tholeiitic volcanic arc basalts (Figure 11 [108], Figures 13 and 14 [110,111]).

**Table 2.** Sm–Nd isotopic data of studied rocks.

Sample/Anal. No	<i>t</i> (Ma)	<sup>147</sup> Sm/ <sup>144</sup> Nd <sub>(0)</sub>	<sup>147</sup> Sm/ <sup>144</sup> Nd <sub>(t)</sub>	<sup>143</sup> Nd/ <sup>144</sup> Nd <sub>(0)</sub>	2σ	<sup>143</sup> Nd/ <sup>144</sup> N <sub>(t)</sub>	T <sub>DM</sub> (Ga)	εNd <sub>(0)</sub>	εNd <sub>(t)</sub>
JAK-1	240.0	0.2317	0.2320	0.513063	0.000005	0.5127	−0.74	8.33	7.26
JAK-2	240.0	0.1959	0.1963	0.513039	0.000005	0.5127	0.95	7.86	7.89
MR-1	240.0	0.2080	0.2084	0.513060	0.000007	0.5127	2.41	8.27	7.93
BRT-1	240.0	0.1857	0.1860	0.512930	0.000006	0.5126	1.20	5.74	6.08
COL-1	240.0	0.2099	0.2103	0.512770	0.000008	0.5124	14.74	2.61	2.21
DO-K-4	240.0	0.2099	0.2103	0.513046	0.000006	0.5127	4.18	8.00	7.60
DO-113	240.0	0.2249	0.2253	0.512956	0.000008	0.5126	−2.66	6.24	5.38
DO-16	250.0	0.1121	0.1123	0.512169	0.000005	0.5120	1.47	−9.11	−6.41
DO-18	240.0	0.1525	0.1527	0.512817	0.000005	0.5126	0.83	3.53	4.89
SUG-10	240.0	0.1721	0.1724	0.512672	0.000006	0.5124	1.75	0.70	1.46
VFK-1	240.0	0.1791	0.1794	0.513030	0.000009	0.5127	0.53	7.69	8.23

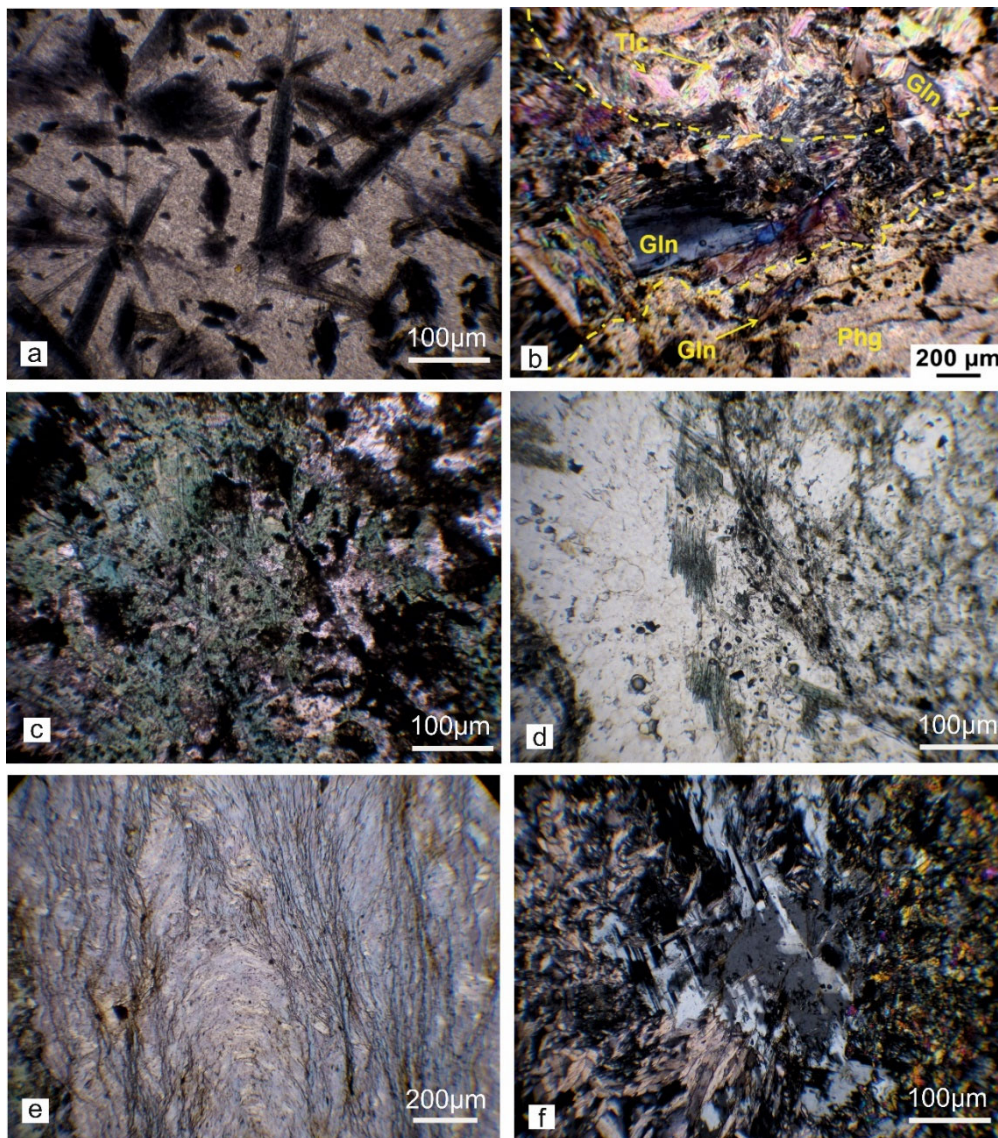


**Figure 9.** Microstructures of Meliatic metabasalts. (a) Gln-Phg-rich blueschist (s. DOL-1) of calc-alkaline basalt protolith. (b) Contact of blueschist (s. DOL-1) with Tlc-Phg-Chl-Cal schist. (c) N-MORB metabasalt (s. DO-K1) with metamorphic Act (needles) to Mg-Rbk (bluish blasts), Chl, Ep and albitized Pl laths. (d) Metamorphic veinlets crosscutting radiolarians-bearing metachert (s. DO-K2, K3) with blue-green Amp-Cal-Chl-Ep aggregates. (e) N-MORB type blueschist (s. MR-1) from below the Malý Radzim Hill at Brdárka. The first and secondary metamorphic cleavage planes are defined by blue Gln. (f) Blueschist of N-MORB (s. MR-1) with layers rich in Ep, Ab, and Gln.

#### 4.3.2. Jaklovce-Velký Folkmár Area Metabasalts

Metabasalts and metadolerites in cherty schists and metaradiolarites still preserve magmatic ophitic and often amygdaloidal textures composed of Cpx and lath-shape Pl, with rare Cr-Spl (Figure 16a,b). They bear the signatures of metamorphic overprinting in networks of veins and veinlets infilled by newly-formed Chl, Ep, Cal, Ab, Act, less Win or Rbk,  $\pm$ Qz (Figure 16c,d, Figures S1 and S2; Table S1). Meanwhile, the metamorphic process in more rigid radiolarites preferably ran in veins and veinlets infilled by the mentioned metamorphic minerals (Figure 16e,f). Rare pelagic carbonates are overgrown by Act-Chl-Ep aggregates (Figure 16g) and the micro-nodules in cherty clayey-carbonatic shales were replaced by metamorphic Amp, Cal, and Ep (Figure 16h). The published estimates established MP greenschist facies metamorphic P–T conditions [70–72] (Figure S1a).

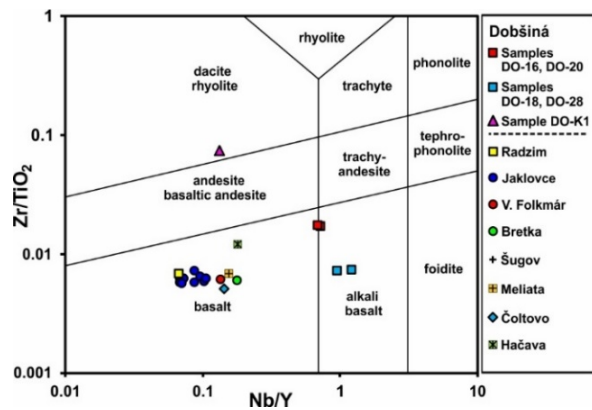


**Figure 10.** Nb/Y–Zr/TiO<sub>2</sub> discrimination diagram of [107] for the Meliatic metabasalts. Xenocryst Zrn most likely caused DO-K1 basalt shift to the rhyolite-dacite field.

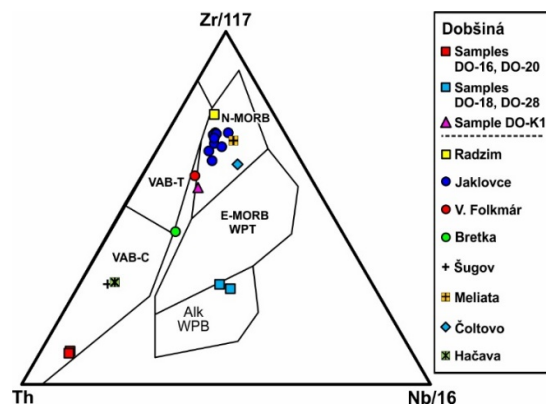


**Figure 11.** Zr/117–Th–Nb/16 discrimination diagram of [108] for the Meliatic metabasalts. Three groups of basalts were distinguished: Calc-alkaline, alkaline, and N-MORB. Abbreviations; alkaline within-plate basalts (Alk WPB), enriched mid-ocean ridge basalts (E-MORB), normal mid-ocean ridge basalts (N-MORB), calc-alkaline volcanic arc basalts (VAB-C), tholeiitic volcanic arc basalts (VAB-T), and within plate tholeiites (WPT).

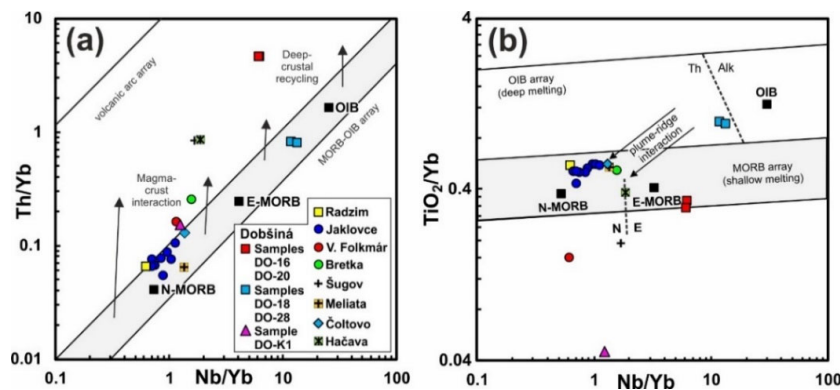


**Figure 12.** Meliatic metabasalts in the Th/Yb versus Nb/Yb and TiO<sub>2</sub>/Yb versus Nb/Yb Proxy discrimination diagrams of [109]. (a) Most N-MORBs remain in the mantle array, thus suggesting subduction-unrelated upper mantle sources. The BRT, DO-K, and VFK N-MORBs may exhibit weak interaction with the crustal rocks from Jurassic subduction. Samples DO-18 and 28 are close to the OIB field. The DO-16, DO-20, SUG, and HAC calc-alkaline basalts may indicate deep-crustal recycling in a volcanic arc. (b) N-MORBs may suggest plume-ridge interaction in the initial stage of a marginal oceanic crust evolution (samples DO-18 and 28). Samples with decreased TiO<sub>2</sub> are outside the OIB and MORB fields.

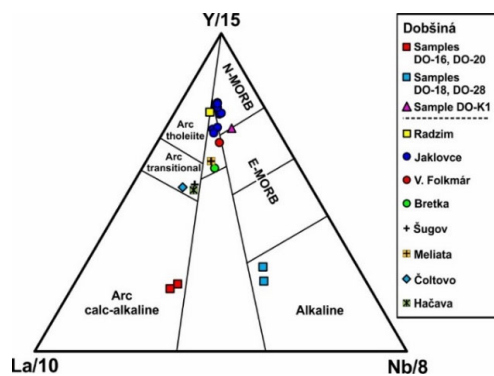


**Figure 13.** Geotectonic origin of the Meliatic metabasalts in diagram of [110]. Three groups of basalts were distinguished: (1) calc-alkaline arc basalts (DO-16, 20), including transitional ones to arc tholeiites (SUG, HAC, COL), (2) alkaline (DO-18, 28), and (3) N-MORB, including N-MORB of BAB (a middle small triangle area).

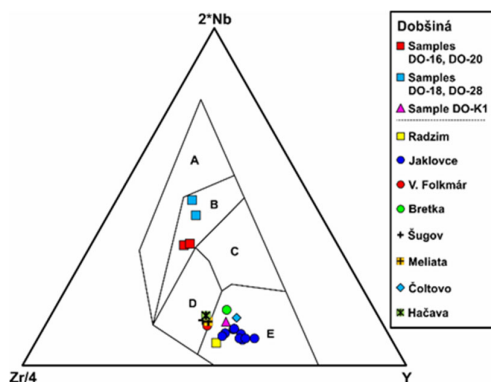


**Figure 14.** Geotectonic discrimination diagram Zr–Nb–Y [111] for the Meliatic metabasalts. The fields are: A1—within plate basalts, B—within plate alkali basalts and within plate tholeiites; C—E-type MORB; D—within plate tholeiites and volcanic arc basalts; and E—N-type MORB and volcanic arc basalts.

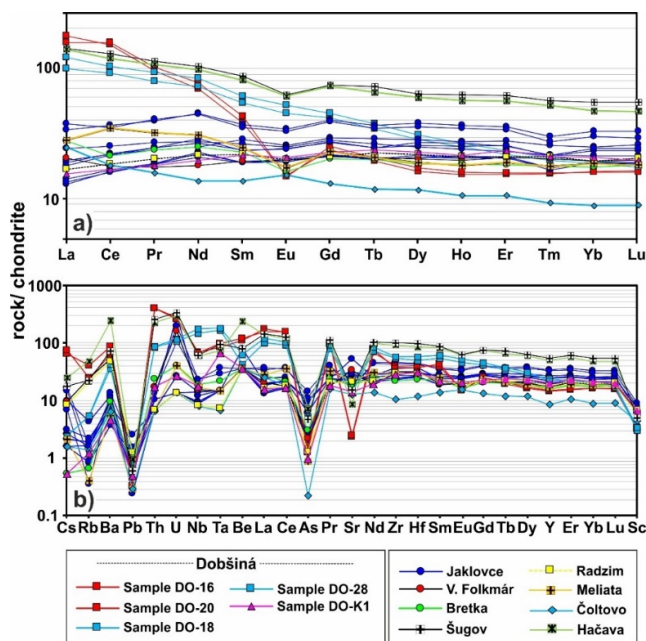


**Figure 15.** (a) Multi-element diagram and (b) Chondrite-normalized REE element patterns of metabasalts from the Meliaticum. Normalizing values are from [116].

Table 1 lists the major elements and this shows that most of the Jaklovce metabasites have basic composition, with SiO<sub>2</sub> contents ranging from 39.63% (1 sample), but mostly from 43.37% to 49.82%. These rocks have clear sub-alkaline nature with very low 0.07 to 0.11 Nb/Y ratios. With the exception of JAK-18 and JAK-22's 2.67–2.95 wt. % TiO<sub>2</sub>, their 1.52–1.97 wt. % TiO<sub>2</sub>, 0.15–0.31 wt. % P<sub>2</sub>O<sub>5</sub>, 87–172 ppm Zr, 31–54 ppm Y and 45–56 Ti/V ratios are very similar to those of modern MORBs [117]. The Nb(Ta)/Yb and Th/Yb values plot along the MORB-OIB array and cluster towards relatively depleted compositions (Figure 12 [109]). These rocks exhibit variable LREE depletion compared to the LREE normalized values of Šugov Valley, Hačava, and some Dobšiná samples (Figure 15; cf. Figure S3). This is evident in their 0.69–1.06 (La/Sm)<sub>N</sub> and 0.79–1.24 (La/Yb)<sub>N</sub> ratios which support their N-MORB affinity, and they also have overall HREE enrichment 19–33 times chondrite abundance and of 6–11 times primitive mantle abundance. The referenced discrimination diagrams (Figure 11 [108], Figure 14 [111]) depict that these basaltic rocks plot in typical N-MORB fields.

Figure 10 highlights that all studied metabasalt to dolerite samples (Figure 10 [107]) are N-MORBs according to chondrite normalized REE patterns ([116]; Figure 15) and other immobile trace elements in Table 1 (Figure 11 [108]) are typical of oceanic crust and particularly back-arc or marginal oceanic basins (Figure 13 [110]). The whole-rock Nd isotopic data (Table 2) of massive to amygdal basalts and dolerites ( $\epsilon\text{Nd}_{240} = 7.26$  and  $7.89$ , JAK-1 and 2 samples, respectively) are consistent with their chondrite-normalized REE patterns (Figure 15; cf. Figure S3), thus indicating a depleted upper mantle source.

The Veľký Folkmár block of Meliaticum is a continuation of the Jaklovce mélangé block towards the SE (Figure 2). The Veľký Folkmár (VFK-1,  $\epsilon\text{Nd}_{240} = 8.23$ , Tables 1 and 2) ophiolitic block shows the MP greenschist facies overprinting (Act, Phg, Ep, Ab) of metabasalts (Figure 6, Figure 16b). This event may have caused a slight enrichment of the sample VFK-1 in LREE (Figure 15) and an eccentric position in the N-MORB fields in discrimination diagrams (Figure 11, Figure 12a, Figure 13, Figure 14). The Veľký Folkmár sample has slightly higher, but still low Nb/Y = 0.14 and very low Zr/TiO<sub>2</sub> = 0.01 ratios (Figure 10 [107]), thus displaying its clear sub-alkaline nature. It is characterized by moderate TiO<sub>2</sub> = 1.97 wt. %, and similarly low Zr = 119 ppm and Y = 27.2 ppm contents. The Ti/V = 63 together with the Nb(Ta)/Yb and Th/Yb values plot the VFK-1 sample in the field for basalts generated at mid-ocean ridge settings [113] or along the MORB–OIB array towards depleted compositions (Figure 12 [109]).

The chondrite-normalized REE pattern is very flat, and the (La/Yb)<sub>N</sub> = 1.1 value is comparable to those with typical N-MORB composition (Figure 15; cf. Figure S3) The overall LREE enrichment is of 21 times the chondrite abundance and of 7 times primitive mantle abundance. In the discrimination diagrams (Figure 11 [108], Figure 14 [111]), this basaltic rock plot in the boundary between N-MORB and tholeiitic volcanic arc basalts.

#### 4.3.3. Other Meliatic Metabasalts (Meliata, Čoltovo, Bretka, Hačava, Šugov Valley)

Some basalt-bearing blocks in the Jurassic sedimentary matrix of mélangé blocks have well preserved magmatic textures. These textures of anchi-metamorphosed Pl-rich basalts are partly preserved in the Meliata (MEL-15) and Čoltovo (COL-1,  $\epsilon\text{Nd}_{240} = 2.21$ , Tables 1 and 2) localities and comprise acicular Ab-Pl aggregates with calcified Cpx phenocrysts. A metabasalt fragment at the Meliata village in sample MEL-15 is present as a very rare olistolith in the Jurassic sediments [4,64].

The Meliata and Čoltovo basaltic samples are generally geochemically similar, while Bretka appears some differences. All of them have slightly higher, but still low Nb/Y (0.14–0.18) and very low Zr/TiO<sub>2</sub> (0.01) ratios (Figure 10 [107]), thus displaying their clear sub-alkaline nature. They are characterized by low to moderate TiO<sub>2</sub> content (0.79–1.62 wt. %), and similarly low Zr (40–113 ppm) and Y (13.2–26.4 ppm) contents. The Ti/V ratio ranges between 51–57, and together with the Nb(Ta)/Yb and Th/Yb values, these plot them in the field for basalts generated at mid-ocean ridge settings [113] or along the MORB–OIB array towards depleted compositions (Figure 12 [109]). The chondrite-normalized REE patterns have slightly increased LREE over MREE and HREE (Figure 15; cf. Figure S3), with

$(La/Sm)_N = 1.2\text{--}1.8$  and  $(La/Yb)_N = 1.5\text{--}2.8$ , and the overall LREE enrichment ranges from 21 to 28 times the chondrite abundance and of 8–9 times primitive mantle abundance. In the discrimination diagrams (Figure 11 [108], Figure 14 [111]), these basaltic rocks plot in the boundary between N-MORB and tholeiitic volcanic arc basalts. In contrast, Figure 13 [110] discrimination diagram has back-arc or arc transitional setting only in the Čoltovo sample. The decreased  $\epsilon Nd_t$  (Table 2) may indicate relatively strong hydrothermal alteration in this rock or a heterogeneous mantle source.

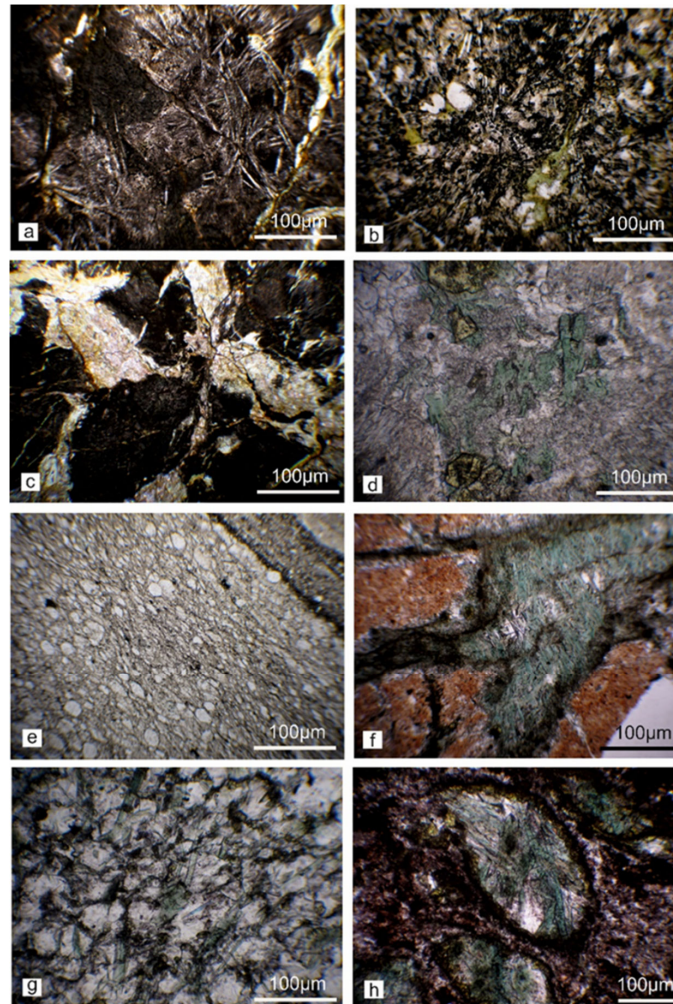


**Figure 16.** Microstructures of rocks from the Jaklovce–Veľký Folkmár area. (a) (s. JAK-1) and (b) (s. VFK-1) examples of well preserved magmatic–ophitic to acicular structures of N-MORBs with Pl laths and tiny relics of Cpx crosscut by metamorphic veinlets. (c) Fragmented metabasalt by metamorphic veinlets. (d) Veinlet infill detail of s. JAK-1 with Cal, Act/Win/Rbk, Ep, Ab, and Chl. (e) Radiolarians-bearing metacherts with Phg-rich (original clayey) laminae (s. JAK-1/3). (f) Metamorphic veinlets crosscutting a metachert (s. JAK-1/2) composed of Amp (Act/Win/Rbk), Ep, Cal,  $\pm Qz$ ). (g) Granoblastic texture of a cherty carbonate enriched in metamorphic Amp aggregates. (h) Micro-nodules in cherty clayey-carbonatic shales (s. JAK-2/1) replaced by metamorphic Amp, Cal, and Ep.

The Bretka locality mélangé comprises metabasalts in association with serpentinites. Part of metabasalt fragments has alternation in some places with dark carbonatic schists (s. BRT-5) and shows the greenschist facies (Chl, Act, Ab, Ep, Czo, Cal) metamorphic overprinting. Other metabasalt fragments are metamorphosed in amphibolite facies (Ed to Prg, Ep, Czo, Ab-Pl, Ttn) crosscut by veinlets composed of greenschist facies mineral assemblages (s. BRT-1,  $\epsilon Nd_{240} = 6.08$ , BRT-2; Table 1, Table 2, Table S1; Figure S1).

Most of the HP metabasalt-bearing blocks, including those from Šugov Valley (s. SUG-10) and Hačava (s. HAC-1), the described Dobšiná block north of Dobšiná town (s. DO-16, 20, DOL-1 samples) and further localities (Jasov, Bôrka) are not ophiolitic (Tables 1 and 2). They contain Gln, Phg, Jd/Ab, Ep  $\pm$  Grt,  $\pm$  Tlc assemblages typical of the Bôrka Nappe [29,30,118]). The Grt blueschists (Figure S4, Table S1) of the Šugov Valley (SUG-10,  $\epsilon\text{Nd}_{240} = 1.46$ , Tables 1 and 2) and Hačava (HAC-1) alternate with pale Middle to Upper Triassic marbles overlying the Permian volcano-sedimentary rocks. The investigated metabasalt samples from Šugov Valley (SUG-10) and Hačava (HAC-1) have low Nb/Y (0.18), low Zr/TiO<sub>2</sub> (0.01) in Hačava and slightly increased Zr/TiO<sub>2</sub> (0.02) ratios (Figure 10 [107]). This places them in a sub-alkaline basalt–basaltic andesite field. In addition, the Šugov sample has moderate TiO<sub>2</sub> content (1.71 wt. %), while Hačava’s is high (2.92 wt. %), and both samples have high Zr (348–385 ppm) and Y (79–85 ppm) contents. The Nb(Ta)/Yb and Th/Yb values plot them on the boundary between basic–intermediate rocks generated in intra-plate volcanic zones and active continental margin settings [114] or between the MORB–OIB and the volcanic arc arrays with relatively enriched compositions. This may indicate magma–crust interaction (Figure 12 [109]). The chondrite-normalized REE patterns exhibit slightly decreasing contents from LREE to HREE (Figure 15; cf. Figure S3), with  $(\text{La}/\text{Sm})_{\text{N}} = 1.6$  to 1.7 and  $(\text{La}/\text{Yb})_{\text{N}} = 2.6$  to 2.96 displaying overall LREE enrichment 141–143 times that in chondrite and of 47–48 times primitive mantle abundance. These samples plot in the calc-alkaline volcanic arc/arc transitional field or within-plate tholeiites (Figure 11 [108], Figure 13 [110], Figure 14 [111]).

#### 4.4. Zircon and Rutile Geochronology Data and Interpretation

##### 4.4.1. Dobšiná Area Mélange Blocks

The early Middle Triassic zircon U–Pb SIMS Concordia age of  $245.5 \pm 3.3$  Ma was determined from a calc-alkaline metabasalt (sample DOL-1, analogous with DO-16 and 20; Figure 17a–c, Table 3, Table S2) in contact with hosting Lower/Middle Triassic(?) carbonate-marly sediments of a Dobšiná mélangé block (Figure 3, Figure 4, Figure 5a, Figure 9a,b).

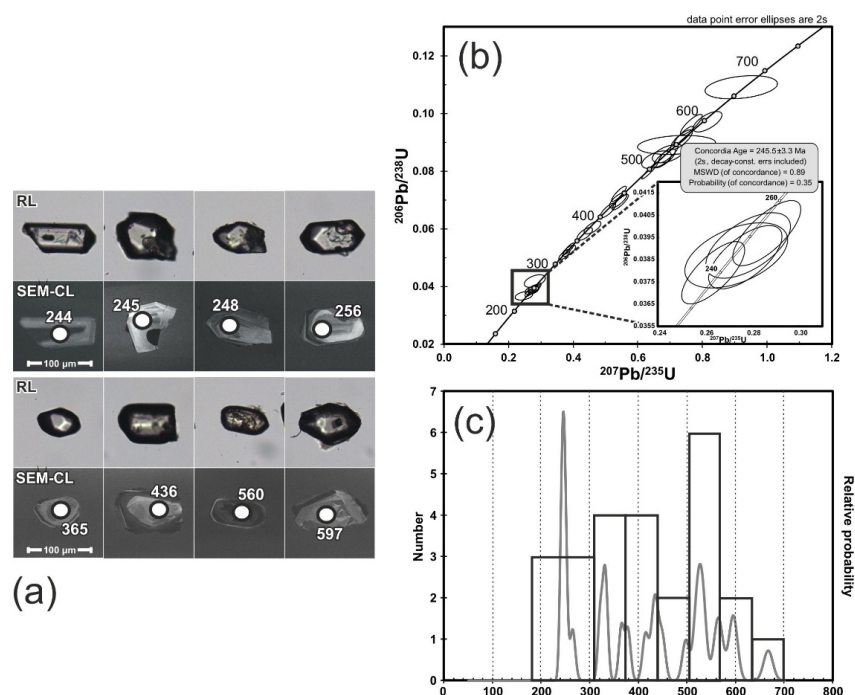


**Figure 17.** (a) Examples of zircon reflected light (RL) and SEM cathode-luminescent (SEM-CL) images from metabasalt s. DOL-1 in the Dobšiná quarry with dated spots. (b) Zircon U–Pb SIMS age diagram. (c) Relative probability and age histograms from s. DOL-1.

Approximately one third of the 47 separated maximum 100  $\mu\text{m}$  Zrn grains from the blueschist-facies metabasalt (Figure 17a) are well shaped, oscillatorily zoned, and often with much higher Th/U ratio from 0.4 to 0.7 compared to older Early Paleozoic or Neoproterozoic Zrn (Table 3). These older Zrn grains, which are rounded due to recycling or a longer distance transport, and moreover often containing inherited cores overgrown by newer Zrn zones are interpreted as the xenocryst Zrn in basalt.

Because of mixing the different Zrn generations and unclear age of hosting sediments, it is not clear whether the youngest identified Zrn population is really own magmatic Zrn of the basalt. We can not exclude the situation, when this Zrn was gained together with the other detrital Zrn populations from non-consolidated Early/Middle Triassic sediments during the basalt emplacement. Such a Zrn population could have been released from a magmatic source (calc-alkaline basalts?) during the advanced continental margin rifting and subsequently transported to the marginal Meliata Basin by turbidites. Triassic acidic rocks are unknown in the IWC. Zircon of this (Anisian) age appeared even as a prevailing detrital Zrn population in biostratigraphically determined Ladinian to Carnian oceanic cherts in the Jaklovce area (Figure 18).

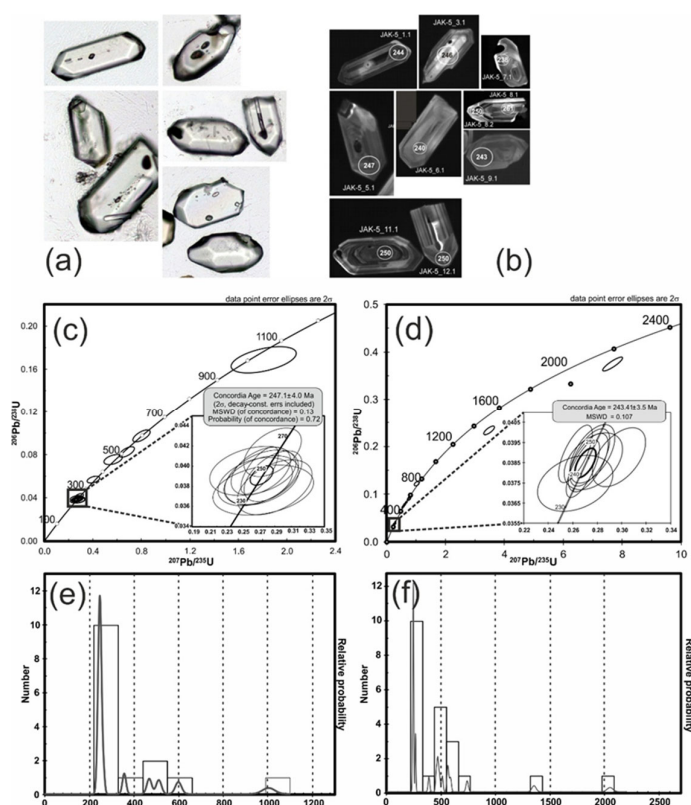


**Figure 18.** (a) Morphology of dated zircon crystals in optical microscope from cherty schist sample JAK-5 (~JAK-1/2 sample layer) in Jaklovce cross-section (see Figure 6, Figure 7, Figure 16). (b) Examples of zircon CL (SEM-CL) images with dated spots from s. JAK-5. (c) Zircon U–Pb SIMS age diagram from cherty schist s. JAK-5. (d) Zircon U–Pb SIMS age diagram from cherty schist s. JAK-5A (~JAK-1/2 s. layer) in Jaklovce cross-section; (a–c) from [72] for comparison with new dated s. JAK-5A. (e) Zircon relative probability and age histograms from cherty schist s. JAK-5. (f) Zircon relative probability and age histograms from cherty schist s. JAK-5A.

#### 4.4.2. Jaklovce Area Mélange Blocks

The detrital zircon U–Pb SIMS ages of  $247 \pm 4$  Ma and  $243 \pm 4$  Ma were determined from the cherty shales (Figure 18a–f, Table 3 and Table S2), and xenocryst Zrn age of  $266 \pm 3$  Ma from an approximately 0.5 m thick basalt layer (Figure 19a–c, Table 3 and Table S2) in the cherty shales (Figure 6, Figure 7b, Figure 16f).

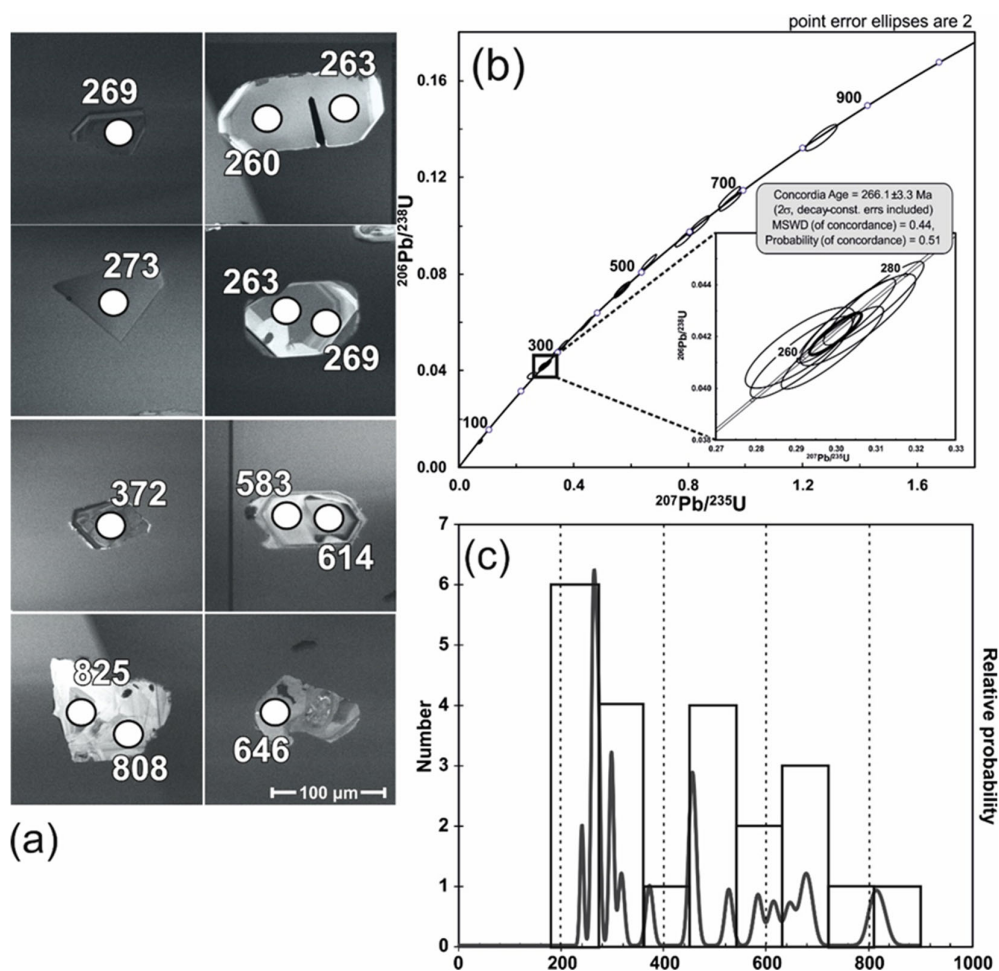


**Figure 19.** (a) Examples of zircon CL (SEM-CL) images from metabasalt sample JAK-1 in Jaklovce cross-section (see Figure 6, Figure 7b,c, Figure 16a) with dated spots. (b) Zircon U–Pb SIMS age diagram from this sample. (c) Relative probability and age histograms from sample JAK-1.

Detrital Zrn grains from the prevailing Triassic Zrn population of cherts have magmatic well-shaped forms and oscillatory zoning, and these indicate an unknown Early/Middle Triassic magmatic source. The older Zrn is Permian, Early Paleozoic, and Neo-Proterozoic, and most likely derived from the Gemic-type basement complexes (cf. [48]) including Permian granites and volcanites [49]. These rocks may have also been the Zrn source for cherty shales and N-MORB extrusions of the peperitic horizons (Figure 7g). The Anisian detrital Zrn ages constrain the maximum Ladinian age of the cherty shales and the N-MORB layer, and it is consistent with the radiolarian stratigraphy of the Lower Beds of the oceanic Jaklovce Succession.

Moreover, the Zrn detritus from the inferred Gemic type Early Paleozoic basement complexes provides characteristic Concordia ages of  $342 \pm 5$ ,  $359 \pm 7$ ,  $488 \pm 7$ , and  $505 \pm 13$  Ma [72].

The U–Pb SIMS metamorphic Rt age from metabasalt sample JAK-1 of approximately 100 Ma (Figure 20a,b, Table 3) most likely indicates reburial/overheating of the Meliatic fragments within the IWC orogenic wedge in the late Early Cretaceous [8,119].

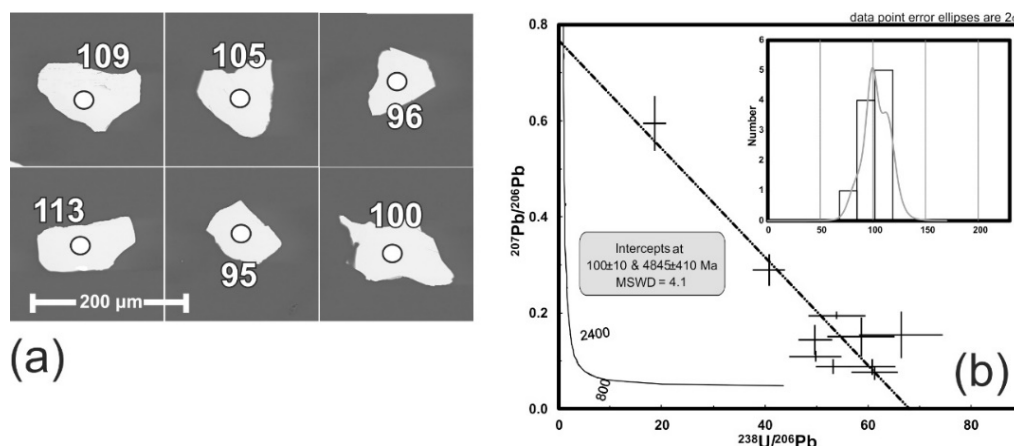


**Figure 20.** (a) Examples of rutile CL (SEM-CL) images from metabasalt s. JAK-1 in Jaklovce cross-section (Figure 6, Figure 7b,c, Figure 16a) with dated spots. (b) Rutile U–Pb SIMS age diagram from this sample.

**Table 3.** Data used in Concordia age Zrn and Rt calculations. An additional set of isotopic data is in Table S2.

Sample/Spot	U	Th/U	f <sub>206</sub>	<sup>207</sup> Pb/ <sup>235</sup> U	±σ	<sup>206</sup> Pb/ <sup>238</sup> U	±σ	ρ	<sup>207</sup> Pb/ <sup>235</sup> U	±σ	<sup>206</sup> Pb/ <sup>238</sup> U	±σ
Zircon	(ppm)		(%)		(%)		(%)		Age (Ma)	(Ma)	Age (Ma)	(Ma)
DOL-1/06	580.4	0.592	0.07	0.2636	2.07	0.0379	1.51	0.73	237.5	4.4	239.9	3.6
DOL-1/10	280.4	0.302	0.11	0.2734	3.26	0.0387	1.55	0.47	245.4	7.1	244.8	3.7
DOL-1/14	441.1	0.243	0.14	0.2785	2.64	0.0391	1.53	0.58	249.5	5.9	247.5	3.7
DOL-1/24	768.3	0.476	0.32	0.2863	2.06	0.0397	1.51	0.73	255.7	4.7	251.0	3.7
DOL-1/31	657.4	0.741	0.01	0.2772	2.29	0.0386	1.50	0.66	248.5	5.1	244.2	3.6
JAK-1/02	1272.0	0.726	0.06	0.3095	1.66	0.0433	1.52	0.91	273.8	4.0	273.2	4.1
JAK-1/17	422.0	0.337	0.10	0.3056	1.93	0.0427	1.69	0.87	270.8	4.6	269.2	4.5
JAK-1/27	1630.1	0.084	0.06	0.3027	1.67	0.0426	1.55	0.93	268.5	3.9	268.9	4.1
JAK-1/06	443.1	1.079	0.20	0.2912	1.92	0.0416	1.54	0.80	259.5	4.4	262.6	4.0
JAK-1/16	509.2	0.659	0.19	0.2992	1.74	0.0416	1.57	0.90	265.8	4.1	262.5	4.0
JAK-1/05	557.0	1.181	0.16	0.2915	1.80	0.0412	1.56	0.87	259.7	4.1	260.3	4.0
JAK-5A/01	762.2	0.390	0.07	0.2620	2.15	0.0389	1.50	0.70	236.3	4.5	246.2	3.6
JAK-5A/02	878.0	0.824	0.10	0.2682	2.10	0.0382	1.53	0.73	241.3	4.5	241.7	3.6
JAK-5A/06	2402.3	0.237	0.07	0.2893	1.72	0.0419	1.50	0.87	258.0	3.9	264.8	3.9
JAK-5A/07	830.4	0.361	0.08	0.3015	2.28	0.0419	1.54	0.68	267.6	5.4	264.4	4.0
JAK-5A/08	264.9	0.374	0.62	0.2620	4.79	0.0375	1.50	0.31	236.3	10.2	237.2	3.5
JAK-5A/10	1074.6	0.698	0.25	0.2738	2.43	0.0388	1.50	0.62	245.8	5.3	245.2	3.6
JAK-5A/18	861.9	0.505	0.61	0.2725	2.45	0.0385	1.55	0.63	244.7	5.3	243.6	3.7
JAK-5A/21	617.6	0.363	1.54	0.2977	3.01	0.0388	1.53	0.51	264.6	7.0	245.2	3.7
JAK-5A/22	802.5	0.093	0.39	0.2760	2.71	0.0389	1.52	0.56	247.5	6.0	246.2	3.7
JAK-5A/23	439.9	0.426	1.36	0.2768	3.51	0.0386	1.50	0.43	248.2	7.7	244.0	3.6

Sample/Spot	U	Th/U	<sup>238</sup> U/ <sup>206</sup> Pb	±σ	<sup>207</sup> Pb/ <sup>206</sup> Pb	±σ	<sup>238</sup> U/ <sup>206</sup> Pb	±σ
Rutile	(ppm)			(%)		(%)	Age (Ma)	(Ma)
JAK-1/06	11.9	0.002	49.8006	3.36	0.1439	10.85	112.7	6.3
JAK-1/07	9.4	0.071	40.7995	3.77	0.2897	5.61	108.6	7.3
JAK-1/08	32.3	0.000	61.4157	3.68	0.0760	9.66	100.4	4.6
JAK-1/09	33.4	0.001	60.8511	3.72	0.0880	9.49	99.8	4.8
JAK-1/10	23.3	0.069	53.9990	5.09	0.1943	1.95	96.5	5.5
JAK-1/11	13.9	0.000	58.7107	5.54	0.1503	13.60	94.8	8.0
JAK-1/16	101.7	0.013	53.3180	3.19	0.0889	8.82	113.7	4.8
JAK-1/17	21.2	0.000	49.8471	5.06	0.1100	4.75	118.1	6.8

## 5. Discussion and Summary of Main Results

### 5.1. Mélange Sources as Indicators of the Meliatic Triassic–Jurassic Paleotectonic Zones

The geological, lithostratigraphical, geochemical, and bio-geochronological criteria used herein enabled determination of three principal Meliatic Superunit paleotectonic zones as the mélange sources:

(1) Continental margin crust; comprises (a) the Permian–Lower Triassic volcano-sedimentary cover rocks: Siliciclastic sediments associated with trachyrhyolites to trachyandesites, calc-alkaline rhyolites, dacites, and basalts overlying the Early Paleozoic basement rocks and (b) the Middle to Upper Triassic/Lower Jurassic (Gemic) slope successions (cf. [2,77]).

(2) Oceanic margin crust; composed of the Middle (Ladinian) to Upper Triassic (Carnian–Norian and younger) pelagic cherty sediments, N-MORBs and rare alkaline OIBs associated with serpentinized and rodingitized, mostly harzburgitic, mantle fragments (cf. [2,4,7,8,77,90–92]).

(3) Transitional zone between the continental and oceanic crust; composed of trench-like upper Lower Jurassic (Toarcian) to lower Middle Jurassic (Bajocian) calciclastic and Middle to lower Upper Jurassic (Bathonian to Oxfordian) siliciclastic turbiditic flysch formations with olistoliths of Triassic carbonates, radiolarites, and rarely of basalts which may have been derived from both continental and oceanic margin zones (cf. [77,85]).

The first *mélange* source is the Bôrka Unit, derived from a distal part of the shelf to slope facial zones [2–4,77]. Their nappe outliers occur throughout the Gemeric and southern part of the Veporic superunits (Figures 1–3, Figure 6). The siliciclastics, slope limestones with shallow-water limestone olistoliths and basalt lava interlayers are metamorphosed to phyllitic and glaucophane schists [29,74,75]. The representative localities are the Bôrka and Hačava village areas and the Šugov Valley (Figure 2).

The second *mélange* source is the Jaklovce Unit which is the most characteristic oceanic or ophiolitic sedimentary–magmatic succession of the Meliaticum. However, the oceanic Jaklovce Succession was more precisely defined using our new biostratigraphic data (Figure 8) which distinguished the Lower (Ladinian), Middle, and Upper (Carnian to Norian?) Beds. Therefore, we recommend use of the Jaklovce Unit for this unique oceanic, although incomplete ophiolitic paleotectonic Meliatic domain. The Middle to Late Triassic meta-ophiolitic fragments achieved a variable degree of metamorphic overprinting before they were tectonically juxtaposed with the Jurassic flysch sediments, the latter as the soft *mélange* matrix besides the serpentinitic (seafloor erosion?) sandstones. This unit typically occurs around the Jaklovce village, but also in a *mélange* block south of Dobšiná town (Figures 3 and 6).

The third *mélange* source is the Meliata Unit, and this includes the Meliata Unit s.s. previously defined by [2,85]. The sole of the calciclastic and siliciclastic flysches might have been extensionally exhumed serpentinized subcrustal mantle separating the thinned distal continental margin and evolving oceanic margin (Figure 21). Thin, magnetite-rich layers in flysch may indicate a serpentinized mantle source. Two different Jurassic successions formed during the contraction-subduction period of the Meliata Basin in the late Early to early Late Jurassic.

An older part of the trench-like Jurassic flysch succession is characterized by calcareous shales (marlstones) interbedded by carbonatic sandstones rich in detrital Ms, Cal, Dol, Pl/Ab, less Tur, and Qz likely of turbiditic origin. This occurs near both Dobšiná town and Jaklovce village (Figures 3–7). The inferred maximum late Early Jurassic age was determined after *Posidonia*-type bivalves located in the Dobšiná quarry calcareous shales. The metamorphic overprinting of these shales is indistinct despite stronger deformation by intra-folial folding and the secondary cleavage formation, boudination of competent sandy layers, Cal mobilization veins or veinlets and formation of the authigenic Ab, Qz, and Chl. There are clear differences in the metamorphic overprinting grade between the MP/LT grade olistoliths or olistostromatic breccia materials and the Jurassic sediments in the *mélange* with indistinct or VLT metamorphic overprinting.

Relatively younger deep-water below the CCD level flysch succession has a dark-grey to black shaly argillaceous-cherty sediments interlayered with the Bathonian to early Oxfordian dark-gray, green and red radiolarites [2,4,77,85]. Thin siliciclastic sandstones rich in detrital Ms, Pl/Ab, less Tur, and Qz, without carbonatic input are most likely of turbiditic origin. This type of siliciclastic flysch formation occurs around the Meliata village type locality, and accompanying very low-grade metamorphic overprinting is hardly recognizable [40]. Olistoliths of the Triassic radiolarites at Meliata village have similar negligible metamorphic overprint and only chalcedonized radiolarians. In contrast, the pale Triassic marble olistoliths from the Meliata quarry have strong metamorphic-deformational overprinting ductile mylonitic structures. It is therefore generally accepted that the Meliata Unit s.s. was not a subducted part of the Meliaticum, but anchimetamorphosed in an accretionary wedge [8,40].

We suggest the use of the Meliata Unit term for this Jurassic deep-water pelagic trench-like succession with pre- and post-metamorphic olistoliths. Fragments derived from the inferred ophiolitic

successions are very rare in the Meliata Unit cross-section [64,85] and only the Middle-Triassic radiolarites without pillow-basalts have been reported [1–4,77,85]. One fragment of an N-MORB (MEL-15 sample in Figure 15) was discovered S of the nearby Licince village during the field mapping [64].

The Middle to lower Upper Jurassic Bathonian–lower Oxfordian flysch succession is overlain by an upper Oxfordian coarsening upward sequence [85]. This most likely heralded the final closure of the Meliata Basin following subduction of thinned continental and oceanic margin fragments including the flysch inferred mantle-type substrate (Figure 21). While some authors report the Middle Jurassic succession as a trench flysch contemporaneous with subduction and accretionary wedge formation [4,76], the deposition of a part of the succession preceded the late Middle to Late Jurassic subduction period and this is consistent with the younger  $^{40}\text{Ar}$ – $^{39}\text{Ar}$  ages [80–82] of the blueschist HP peak phengite (160–150 Ma). The flysch formation started during a contraction period and this calciclastic flysch age was determined to Toarcian–Bajocian (~180–168 Ma) according to Posidonia-type bivalves from Dobšiná. The deeper-water siliciclastic Bathonian–lower Oxfordian (~167–160 Ma) radiolarians-bearing flysch succession [85] may reflect the flysch basin deepening during the main Middle to early Late Jurassic subduction period.

This trench-like flysch intra-oceanic sedimentary facies may be related to the Neotethyan compression phase recognized throughout the Neotethyan domains of the Southern Alps, Dinarides, and Pelso areas [10]. This phase is a Middle Jurassic intra-oceanic subduction event and north-west obduction of the Triassic ophiolitic sheets [10]. The Meliata Unit flysch basin has a fore-arc/foreland basin position in the relationship to NW-ward ophiolitic Jaklovce Unit nappe transport or a trench-like (supra-subduction) position in relationship to the Middle to Late Jurassic subduction of the Bôrka Unit (Figure 21).

## 5.2. Geochemical Constraints on the Meliatic Basalts Paleotectonic Setting

Geochemical data from the Meliatic basaltic rocks show at least three principal protoliths from three different paleo-tectonic settings (Figures 10–15).

(1) The calc-alkaline basalts have enriched LREE content and depleted HREE content with pronounced Eu anomaly (Figure 15) and this reveals genesis bound to fractional crystallization. The basalts also have Ta, Nb, and Ti depletion, thus suggesting that their mantle source was already depleted in these elements from previous or contemporaneous melt extraction events ([120] and Figures 10–14). These basalts' interaction with crustal sources is compatible with their negative to lower positive  $\epsilon\text{Nd}_t$  values (DO-16, SUG-10, Table 2), and most are incorporated in the Bôrka Nappe derived from the Bôrka Unit with predominant blueschist facies metamorphics [29,78,79].

(2) The alkaline basalts have slight LREE enrichment, slight HREE depletion and they lack Eu anomaly. This emphasizes their primitive source (Iherzolite origin?) and the absence of plagioclase in the early crystallization process. This is consistent with their distinctly positive  $\epsilon\text{Nd}_t$  values (DO-18, Table 2). The REE and many incompatible element ratios, including those for Th/Yb, Nb/Yb, Ta/Yb in Table 1, are quite similar to those observed in typical ocean island basalts [121,122]. This suggests that these rocks' magmas in the Dobšiná mélangé block may have originated from a partly melted plume-type source and are an early stage of the oceanic rifting and ridge-spreading inferred from the Jaklovce Unit (Figure 12b).

(3) The N-MOR basalts are bound only to the Jaklovce Unit, as revealed by the geochemical study (Figures 11–14, Table 1). This unit has ophiolitic blocks in the mélangé in areas south of Dobšiná (DO-K), below the Malý Radzim Hill (MR) west of Brdárka and near Jaklovce (JAK), Veľký Folkmár (VFK), Meliata (MEL), Čoltovo (COL), and Bretka (BRT). Table 2 highlights that they have typically higher positive  $\epsilon\text{Nd}_t$  values. However, the COL-1 sample is rich in Pl and this may indicate a heterogeneous mantle source. Their metamorphic overprinting varies from very low-grade greenschist facies to greenschist, and the discovery of only MR-1 sample indicates that they rarely vary to blueschist

facies. These blocks are usually associated with cherty shales and radiolarites and they finally occur in indistinctly metamorphosed Jurassic sediments (Figure 21).

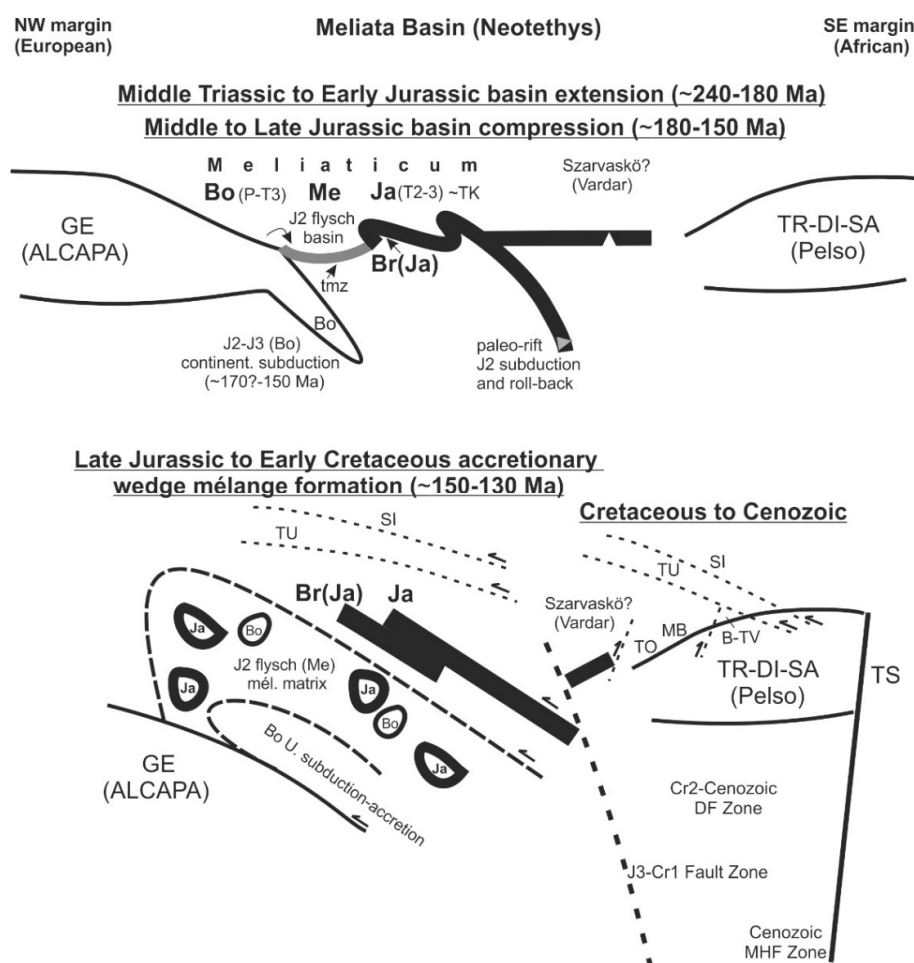


**Figure 21.** Paleotectonic zones and an outline of subduction–accretion structure of the Meliaticum (Meliata Superunit), not to scale. N–S distribution of the Triassic–Jurassic paleotectonic zones: GE—Gemicum (Gemic Superunit—Early Paleozoic basement and Carboniferous–Lower Triassic cover), Bo—the Bôrka Unit continental margin fragments. Me—the Meliata Unit trench-like Jurassic sediments on inferred transitional mantle zone (tmz) separating the continental and oceanic margin crust, Ja—the Jaklovce Unit Middle to Late Triassic oceanic fragments. Br(Ja)—the Bretka ophiolite nappe sole of the Jaklovce Unit. TK—Tornakápolna Triassic ophiolite complex (NE Hungary), TU—Turnaicum, SI—Silicum, TO—Telekesoldal and MB—Mónosbél nappes with the Szarvaskő type Jurassic ophiolites and flysch, B-TV—Bódva-Telekesvölgy T–J series. TR-DI-SA—the Transdanubian Range–Dinaridic–Southern Alps type basement, DF—Darnó Fault, MHF—Mid-Hungarian Fault, TS—the Tisia Microplate, ALCAPA—the Alps-Carpathian-Pannonia Microplate. Arcuate arrow—scraping-off zone and turbidite transport direction. Half-arrow—kinematics of the exhumation and thrusting in an accretionary wedge.

Figure 15 and Figure S3 highlight that the trace element concentrations and LREE/HFSE and LILE/HFSE signatures suggest that most of these N-MORBs originated in a mid-ocean ridge setting without the influence of enriched OIB-type- or subduction-related components. Additional features supporting this suggestion are that the Th versus Nb values have no Nb enrichment compared to Yb [109] and other incompatible elements [122–128]. Similar metabasalts with N-MORB composition and only slight  $(Ce/Yb)_N = 0.9–1.7$  and  $(La/Sm)_N = 0.6–0.9$  fractionation were documented from the

Folkmár Zone [5]. Almost complete lack of a sheeted-dyke and gabbroic layers infers a marginal oceanic basin with incomplete ophiolites.

The abyssal type harzburgites in the Jaklovce Unit ophiolite complex, having a character of weakly depleted harzburgites are consistent with the marginal basin with the subduction-unrelated mantle rocks [7,90–94]. They are also typical of the mantle portion of the ophiolitic complexes [93,94] from the passive margins reported by [129], and which evolved during rift-drift and seafloor spreading [130]. Moreover, the rodingite dykes cross-cutting serpentinitized harzburgites may already have formed on the ocean floor [92]. While the relict homogeneous massive rodingite  $\epsilon\text{Nd}_{240} = 5.38$ ; sample DO-113 in Tables 1 and 2 is predominantly composed of H-Grs, H-Adr, and Chl, the Prv dating from a reaction zone of serpentinite and a massive inferred original rodingite dyke is Early Cretaceous at approximately 135 Ma and therefore constrains the exhumation of these metarodingites from the Meliatic accretionary wedge [8,73,92]. Extensionally exhumed sub-crustal mantle rocks might have formed a sole of the Middle Jurassic trench-like flysch basin (Figure 21).

### 5.3. Evolutionary Model of Meliaticum from Lithology, Geochemistry and Bio-Geochronological Data

Integrated bio and geochronology investigation brought new results which could be applied for a tentative Meliaticum evolutionary model (Figure 21). The Neotethyan back-arc basin model, proposed for the Meliaticum by authors [8,12,15–17] and many others, is doubtful because the Meliaticum was most likely paleogeographically far W of the inferred Paleotethyan active margin in Permian–Triassic, and separated from the southern margin by a large Neotethyan ocean [10].

#### 5.3.1. Middle Triassic to Early Jurassic Extension Basin Period (~240–180 Ma)

The Permian calc-alkaline volcanism identified in the IWC continental crust units [47,49,53,57–60] may have geodynamically preceded the formation of subsequent early Middle Triassic magmatics, the Zrn of which we established from deep-water sediments of the Meliata Basin continental and oceanic margin successions. The youngest Zrn population found in basalt sample DOL-1 from the Dobšiná quarry (Figure 3, Figure 4, Figure 5a,b, Figure 9a,b) was dated to  $245.5 \pm 3.3$  Ma by U–Pb SIMS (Figure 17a–c), and this is interpreted as the magmatic crystallization age of these basalts. Anyway, it constrains the maximum age of hosting sediments to the late Anisian. Alternatively, the calc-alkaline character of basalt samples DO-16, 20 and DOL-1 (Figures 10–15) may suggest a (re)melted Early Paleozoic active continental margin crust during the early Middle Triassic extension and then the discussed Zrn is inherited from a protolith. There is also clear host sediment input of external older Zrn populations to the unconsolidated basaltic melt.

The sedimentation of early Middle Triassic cherty carbonates and shales on a subsiding thinned (Gemic-type) continental margin is interpreted as an advanced continental margin rifting stage and the formation of the marginal Meliata Basin of a large Neotethys Ocean. This event clearly exceeds the inferred Permian active continental margin of a Paleotethyan ocean [12,15–17], and therefore the Permian–Triassic super-plum area generation could be imposed from such an intensive whole-Permian magmatic activity in the IWC Variscan basement complexes. The plum generation could be related to the subducted Devonian to Carboniferous Paleotethyan oceanic and continental margin crust, and the existence of “hot lines” is inferred by some authors [46,49]. Continual overheating from the Late Permian to Triassic is also indicated by the EPMA determined newly-formed Mnz ages of 250–225 Ma in the Gemic basement Permian granites, or in the outer zones of magmatic Mnz in these granites from the inferred Meliatic northern continental margin [49].

The onset of the oceanic rifting stage of the Meliata Basin initiated the formation of greenish and reddish pelagic cherty shales (s. JAK 1/3; Figure 6, Figure 7a, Figure 16e). These had rare thin cherty carbonate and basaltic tuff layers, and herein we document Ladinian radiolarians in the Lower Beds of the oceanic Jaklovce Succession for the first time (Figure 8, images 1–9). Although, this age was inferred from lithological similarities with other Meliatic occurrences [4,68,69]. The basalt samples DO-18 and DO-28 have alkaline character and may come from a paleo-rift from an early stage of the oceanic crust

formation of this marginal oceanic basin (Figure 21). This alkaline basalt type geochemistry shown in Figures 10–15 could be related to a mantle plum upwelling indicated in Figure 12b.

The evolving oceanic rifting stage is recorded by N-MOR-type basalt layers in the Ladinian to Carnian cherts, or by the cherty interlayers enclosed in the basalts often forming peperitic breccias (Figure 6, Figure 7g). Herein, we also document Ladinian to Carnian radiolarians from the Middle (s. JAK-1/2) and Upper (s. JAK-2/1) Beds of the oceanic Jaklovce Succession of the Jaklovce Unit for the first time (Figure 6, Figure 7b,d, Figure 8—images 10–23, Figure 16f–h).

Figure 18a–f shows the detrital Zrn U–Pb SIMS Concordia ages of  $247 \pm 4$  Ma and  $243 \pm 4$  Ma from the cherty shales (s. JAK-5A~JAK-1/2), and Figure 19a–c records the Zrn xenocryst population Concordia age of  $266 \pm 3$  Ma from a 0.5 m thick N-MOR basalt layer (s. JAK-1) in the cherty shales. These reveal continuing connection of the evolving oceanic basin with an adjacent rifted continental margin Permian to early Middle Triassic Zrn magmatic sources. Rhyolitic and “keratophyric” (trachyadacites to trachyandesites in the TAS diagram [131]) clastogeneous to blocky materials of unknown age (Permian to Middle Triassic) were reported from the Jurassic olistostromatic conglomerates and sandstones at the Meliata [4] and Jaklovce [132] villages and also from the Držkovce (DRŽ-1, [133]) and Brusník (BRU-1, [63]) boreholes which could also be their source. Similar and younger ages of the Ladinian to Carnian magmatic activity of 242–227 Ma were reported from the Southern Alps [134]) and also from the Transdanubian Range [35,135] areas from the inferred opposite side of the Neotethys Ocean.

### 5.3.2. Middle to Late Jurassic Subduction, Basin Closure and Accretionary Wedge Mélange Formation (~180–130 Ma)

Southward subduction began in the Middle Jurassic, and the buoyant Jurassic trench-like flysch sediments may have lost their denser sole “transitional” crust during subduction of the distal continental and marginal oceanic crust (Figure 21). Part of the ophiolitic fragments (MEL, COL samples) emplaced in the Jurassic sediments are most likely olistoliths scraped off the marginal oceanic crust during the initial contraction regime in the late Early Jurassic. This is an upper age limit of the trench-like flysch sediments according to *Posidonia-type* bivalves.

Fragments from the continental margin Bôrka Unit (DO-16, 20, DOL-1, SUG-10, HAC-1 samples) and the oceanic margin Jaklovce Unit (MR-1, DO-18, 28 samples) were subducted to a HP depth and these were tectonically juxtaposed with the Jurassic flysch sediments of the accretionary wedge after their exhumation from a subductional channel at approximately 150–130 Ma [8]. The subductional bending of the northern segment of the Meliatic oceanic crust below its southern segment in an inferred mechanically weakened paleo-rift zone may have then caused the intra-oceanic Middle to Late Jurassic volcanic arc (Szarvaskő?) formation which defines the expansion of the Neotethyan Vardar Ocean to the south (Figure 21).

Subductional burial of the ophiolitic Jaklovce Unit fragments with the JAK, DO-K, BRT, and VFK samples to MP depths is constrained by the MP/LT metamorphic assemblages composed of Chl, Act, Win, Rbk, Ttn, Ep, Cal, Qz, and Phg (Figure 9c,d, Figure 16a–h, Figures S1 and S2; Table S1).

Similarly, the Meliata Unit Jurassic flysch with the rare metabasalts (MEL-15 and COL-1 samples) have only a slight anchimetamorphic overprinting [4,40].

The investigated Jaklovce, Velký Folkmár and the Dobšiná DO-K sample fragments have distinctly higher grade MP/LT metamorphic overprinting than the Jurassic flysch sediments. We consider that these are post-subduction olistoliths because they occur as metamorphosed fragments in maximally anchimetamorphosed flysch calcareous shales. Examples of this include the exhumed Bôrka Unit HP (DO-16, DO-20, DOL-1), the Jaklovce Unit HP (MR-1 and DO-18, 28), and other MP (DO-K, JAK, VFK) fragments which were finally tectonically juxtaposed with the Jurassic sedimentary succession of the Meliata Unit as the mélange matrix (Figure 21).

The metamorphic overprinting grade of the Meliatic subduction-related accretionary wedge is mostly in the MP greenschist- to HP blueschist facies (see also [8,29,70–75] and Figures S1, S2, S4; Table S1). The unsubducted to shallowly subducted parts have maximum anchimetamorphic overprinting [1,2,4,8,

30,64,76,77], with the exception of some Bretka N-MORB fragments metamorphosed in the amphibolite facies (BRT-1, 2, 8 samples; Figures S1 and S2; Table S1). This may indicate the metamorphic sole position of this part of the Jaklovce Unit during the NW-ward thrusting of the ophiolite sheets over the Meliata Unit flysch and the exhumed Bôrka Unit fragments (Figure 21). The inferred tectonostratigraphy of an accretionary wedge may be partly preserved in a superposition of larger blocks in the Meliatic mélange, for example at Dobšiná or Jaklovce.

Formation of the Meliatic subduction-related accretionary wedge mélange followed the closure of the Meliata Basin in the Late Jurassic. This process lasted until the Early Cretaceous [8] and was accompanied by a strong tectonization of the rapidly exhuming and cooling wedge fragments. This featured the mylonitization and cataclasis shown in Figure 5c–e. The Zircon (U–Th)/He ages of these fragments from approximately 130 to 100 Ma [8] and the metamorphic rutile U–Pb SIMS age of ca. 100 Ma from the s. JAK-1 Jaklovce metabasalt (Figure 20, Table 3) limit the ages of the mélange formation. This latter age also indicates incorporation of the frontal Meliatic nappe outliers in the IWC orogenic wedge [8]. In addition, the Meliaticum was cross-cut by a system of transpressional faults [34,35] which were active from the Latest Jurassic to Early Cenozoic (Figure 21). This made reconstruction extremely difficult.

In conclusion, the outlined tentative Meliaticum evolutionary model in Figure 21 concurs with a paleogeographic model of a rifted large Neotethys Ocean NW passive continental margin [10]. The intra-oceanic southward subduction of the Meliata Unit ophiolite complex may have led to the formation of the BAB Jurassic Szarvaskő ophiolites [34,37] which were already part of the Jurassic–Cretaceous Neotethyan Vardar Ocean [10] (Figure 21). Finally, the Szarvaskő Unit was displaced by the Telekesoldal and Mónosbél nappes of north-east Hungary, thus suggesting their Dinaridic origin [34,37], and this is supported by similar displaced units including the Turnaicum and Silicicum which overlie the Meliaticum.

**Supplementary Materials:** The following are available online at <http://www.mdpi.com/2075-163X/9/11/652/s1>. Figure S1: (a) Diagram of amphiboles composition in the glaucophane/riebeckite-tremolite/actinolite-tschermakite ternary system after [136] for Dobšiná and Jaklovce metabasalts. (b) Classification diagram of amphiboles after [137] from Bretka metabasalts. Analyses in Table S1. Figure S2: Classification diagram of white mica after [138] from Dobšiná, Jaklovce and Hačava metabasalts. Analyses in Table S1. Figure S3: REE element (a) and Multi-element (b) Primitive mantle normalized patterns of Meliatic metabasalts. Normalizing values are from [116]. Figure S4: Classification diagram of garnet (in association with Gln and Phg) with almandine+pyrope (Alm + Prp), grossular (Grs) and spessartine (Sps) endmembers showing garnet composition from Hačava metabasalts. Analyses in Table S1. Table S1: Representative analyses of amphibole, white mica and garnet from Jaklovce, Dobšiná and Hačava. Table S2: Additional set of zircon U–Pb isotopic data for age calculation diagrams.

**Author Contributions:** Field investigation, M.P., P.R. and Z.N.; methodology, J.S., Q.-L.L., X.-H.L., Z.H., software X.L., Z.H., O.N.; validation, M.O. and M.P.; formal analysis, O.N.; resources, P.R.; data curation, M.O., O.N.; writing—original draft preparation, M.P. (J.S. and M.O.); writing—review and editing, Z.N.; supervision and funding, M.P., Q.-L.L., X.-H.L., Z.H.; project administration, M.P., X.L., Z.H.

**Funding:** This research was funded by the National Key Research and Development Program of China (2016YFE0203000) and the Slovak Research and Development Agency (contracts APVV-15-0050, APVV-17-0017), and VEGA Agency (No. 2/0034/16, No. 1/0151/19).

**Acknowledgments:** Constructive reviews of three reviewers are greatly appreciated. We thank H.-J. Gawlick and A. Vozárová for fruitful discussions; R. Marshall for reviewing the English content, Dana Troppová is thanked for zircon and rutile separation and radiolarians extraction, and J. Li for zircon and rutile mounting for SIMS dating.

**Conflicts of Interest:** The authors declare no conflict of interest. The funders had no role in the design of the study; in the collection, analyses, or interpretation of data; in the writing of the manuscript, or in the decision to publish the results.

## References

1. Kozur, H.; Mock, R. Zum Alter und zur tektonischen Stellung der Meliata-Serie des Slowakischen Karstes. *Geol. Zbor. Geol. Carpath.* **1973**, *24*, 365–374.
2. Kozur, H.; Mock, R. Erster Nachweis von Jura in der Meliata-Einheit der südlichen Westkarpaten. *Geol. Paläont. Mitt. Innsbruck* **1985**, *13*, 223–238.

3. Kozur, H. The evolution of the Meliata–Hallstatt Ocean and its significance for the early evolution of the Eastern Alps and Western Carpathians. *Palaeogeogr. Palaeoclimatol.* **1991**, *87*, 109–135. [[CrossRef](#)]
4. Mock, R.; Sýkora, M.; Aubrecht, R.; Ožvoldová, L.; Kronome, B.; Reichwalder, P.; Jablonský, J. Petrology and petrography of the Meliaticum near the Meliata and Jaklovce villages, Slovakia. *Slovak Geol. Mag.* **1998**, *4*, 223–260.
5. Faryad, S.W.; Spišiak, J.; Horváth, P.; Hovorka, D.; Dianiška, I.; Józsa, S. Petrological and geochemical features of the Meliata mafic rocks from the sutured Triassic oceanic basin, Western Carpathians. *Ofioliti* **2005**, *30*, 27–35.
6. Kovács, S.; Sudar, M.; Karamata, S.; Haas, J.; Peró, C.; Grădinaru, E.; Gawlick, H.-J.; Gaetani, M.; Mello, J.; Polák, M.; et al. Triassic environments in the Circum-Pannonian Region related to the initial Neotethyan rifting stage. In *Variscan and Alpine Terranes of the Circum-Pannonian Region*; Vozár, J., Ebner, F., Vozárová, A., Haas, J., Kovács, S., Sudar, M., Bielik, M., Péró, C., Eds.; Geological Institute SAS: Bratislava, Slovakia, 2010; pp. 87–156.
7. Putiš, M.; Koppa, M.; Snárska, B.; Koller, F.; Uher, P. The blueschist-associated perovskite–andradite-bearing serpentinitized harzburgite from Dobšiná (the Meliata Unit), Slovakia. *J. Geosci.* **2012**, *57*, 221–240. [[CrossRef](#)]
8. Putiš, M.; Danišík, M.; Ružička, P.; Schmiedt, I. Constraining exhumation pathway in an accretionary wedge by (U-Th)/He thermochronology—Case study on Meliatic nappes in the Western Carpathians. *J. Geodyn.* **2014**, *81*, 80–90. [[CrossRef](#)]
9. Gawlick, H.-J.; Missoni, S. Middle Triassic radiolarite pebbles in the Middle Jurassic Hallstatt Mélange of the Eastern Alps: implications for Triassic–Jurassic geodynamic and palaeogeographic reconstructions of the western Tethyan realm. *Facies* **2015**, *61*. [[CrossRef](#)]
10. Gawlick, H.-J.; Missoni, S. Middle-Late Jurassic sedimentary mélange formation related to ophiolite obduction in the Alpine-Carpathian-Dinaridic Mountain Range. *Gondwana Res.* **2019**, *74*, 144–172. [[CrossRef](#)]
11. Csontos, L.; Vörös, A. Mesozoic plate tectonic reconstruction of the Carpathian region. *Palaeogeogr. Palaeoclimatol. Palaeoecol.* **2004**, *210*, 1–56. [[CrossRef](#)]
12. Golonka, J. Plate tectonic evolution of the southern margin of Eurasia in the Mesozoic and Cenozoic. *Tectonophysics* **2004**, *381*, 235–273. [[CrossRef](#)]
13. Handy, M.R.; Schmid, S.M.; Bousquet, R.; Kissling, E.; Bernoulli, D. Reconciling plate-tectonic reconstructions of Alpine Tethys with the geological-geophysical record of spreading and subduction in the Alps. *Earth Sci. Rev.* **2010**, *102*, 121–158. [[CrossRef](#)]
14. Handy, M.R.; Ustaszewski, K.; Kissling, E. Reconstructing the Alps–Carpathians–Dinarides as a key to understanding switches in subduction polarity, slab gaps and surface motion. *Int. J. Earth Sci.* **2015**, *104*, 1–26. [[CrossRef](#)]
15. Stampfli, G.M. The Intra-Alpine terrain: A Paleotethyan remnant in the Alpine Variscides. *Eclogae Geol. Helv.* **1996**, *89*, 13–42.
16. Stampfli, G.M.; Borel, G.D.; Marchant, R.; Mosar, J. Western Alps geological constraints on western Tethyan reconstructions. *J. Virtual Explorer* **2002**, *8*, 77–106. [[CrossRef](#)]
17. Stampfli, G.M.; Kozur, H. Europe from the Variscan to the Alpine cycles. In *European Lithosphere Dynamics*; Gee, D.G., Stephenson, R., Eds.; Geological Society London Memoirs: London, UK, 2006; Volume 32, pp. 57–82.
18. Lexa, J.; Bezák, V.; Elečko, M.; Eliáš, M.; Konečný, V.; Less, G.; Mandl, G.W.; Mello, J.; Pálenský, P.; Pelikán, P.; et al. *Geological Map of Western Carpathians and Adjacent Areas 1:500,000*; Geological Survey of Slovak Republic: Bratislava, Slovakia, 2000.
19. Putiš, M. Tectonic styles and Late Variscan–Alpine evolution of the Tatric–Veporic crystalline basement in the Western Carpathians. *Zent. für Geologie und Paläontologie* **1991**, *1*, 181–204.
20. Putiš, M. Geology and petrotectonics of some shear zones in the West Carpathian crystalline complexes. *Miner. Slov.* **1991**, *3*, 459–473.
21. Putiš, M.; Ivan, P.; Kohút, M.; Spišiak, J.; Siman, P.; Radvanec, M.; Uher, P.; Sergeev, S.; Larionov, A.; Méres, Š.; et al. Metaigneous rocks of the West-Carpathian basement, Slovakia: Indicators of Early Paleozoic extension and shortening events. *B. Soc. Geol. Fr.* **2009**, *180*, 461–471. [[CrossRef](#)]
22. Putiš, M.; Danišík, M.; Siman, P.; Nemeč, O.; Tomek, Č.; Ružička, P. Cretaceous and Eocene tectono-thermal events determined in the Inner Western Carpathians orogenic front Infratatricum. *Geol. Q.* **2019**, *63*, 248–274.

23. Plašienka, D.; Grecula, P.; Putiš, M.; Kováč, M.; Hovorka, D. Evolution and structure of the Western Carpathians: An overview. In *Geological Evolution of the Western Carpathians*; Grecula, P., Hovorka, D., Putiš, M., Eds.; Mineralia Slovaca: Bratislava, Slovakia, 1997; pp. 1–24i.
24. Haas, J.; Kovács, S.; Krystyn, L.; Lein, R. Significance of Late Permian-Triassic facies zones in terrane reconstructions in the Alpine-North Pannonian domain. *Tectonophysics* **1995**, *242*, 19–40. [[CrossRef](#)]
25. Janik, T.; Grad, M.; Guterch, A.; Vozár, J.; Bielik, M.; Vozárová, A.; Hegedüs, E.; Kovács, C.A.; Kovács, I.; Keller, G.R. Crustal structure of the Western Carpathians and Pannonian Basin: Seismic models from CELEBRATION 2000 data and geological implications. *J. Geodyn.* **2011**, *52*, 97–113. [[CrossRef](#)]
26. Hovorka, D.; Jaroš, J.; Kratochvíl, M.; Mock, R. The Mesozoic ophiolites of the Western Carpathians. *Krystalinikum* **1984**, *17*, 143–157.
27. Ivan, P. Relics of the Meliata Ocean crust: Geodynamic implications of mineralogical, petrological and geochemical proxies. *Geol. Carpath.* **2002**, *53*, 245–256.
28. Reichwalder, P. Geologische Verhältnisse des jüngeren Paläozoikums im SÖ Teil des Zips-Gemerer Erzgebirges. *Západné Karpaty* **1973**, *18*, 99–139.
29. Faryad, S.W. Phase petrology and P-T conditions of mafic blueschists from the Meliata unit, Western Carpathians, Slovakia. *J. Metamorph. Geol.* **1995**, *13*, 701–714. [[CrossRef](#)]
30. Mello, J.; Reichwalder, P.; Vozárová, A. Bôrka Nappe: High-pressure relic from the subduction-accretion prism of the Meliata Ocean (Inner Western Carpathians, Slovakia). *Slovak Geol. Mag.* **1998**, *4*, 261–274.
31. Réti, Z. Triassic ophiolite fragments in an evaporitic mélange, Northern Hungary. *Ofioliti* **1985**, *10*, 411–422.
32. Kovács, S. Major events of the tectono-sedimentary evolution of the North Hungarian Paleo-Mesozoic: History of the Northwestern termination of the Late Paleozoic-Early Mesozoic Tethys. In *Tectonic Evolution of the Tethyan Region*; Sengör, A.M.C., Ed.; Kluwer Acad. Press: Dordrecht, The Netherlands, 1989; pp. 93–103.
33. Horváth, P. Metamorphic evolution of gabbroic rocks of the Bódva Valley ophiolite complex, NE Hungary. *Geol. Carpath.* **2000**, *51*, 121–129.
34. Kövér, S.; Fodor, L.; Judik, K.; Németh, T.; Balogh, K.; Kovács, S. Deformation history and nappe stacking in Rudabánya Hills (Inner Western Carpathians) unravelled by structural geological, metamorphic petrological and geochronological studies of Jurassic sediments. *Geodin. Acta* **2009**, *22*, 3–29. [[CrossRef](#)]
35. Kövér, S.; Fodor, L.; Kovács, Z.; Klötzli, U.; Haas, J.; Zajzon, N.; Szabó, C. Late Triassic acidic volcanic clasts in different Neotethyan sedimentary mélanges: Paleogeographic and geodynamic implications. *Int. J. Earth Sci.* **2018**, *107*, 2975–2998. [[CrossRef](#)]
36. Zajzon, N.; Váczi, T.; Fehér, B.; Takács, Á.; Weiszbürg, T.G. Pyrophanite pseudomorphs after perovskite in Perkupa serpentinites (Hungary): A microtextural study and geological implications. *Physics Chem. Miner.* **2013**, *40*, 611–623. [[CrossRef](#)]
37. Kiss, G.B.; Oláh, E.; Zaccarini, F.; Szakáll, S. Neotethyan rifting-related ore occurrences: Study of an accretionary mélange complex (Darnó Unit, NE Hungary). *Geol. Carpath.* **2016**, *67*, 105–115. [[CrossRef](#)]
38. Dosztály, L.; Józsa, S. Geochronological evaluation of Mesozoic formations of Darnó Hill at Reck on the basis of radiolarians and K-Ar data. *Acta Geol. Hungar.* **1992**, *35*, 371–394.
39. Kiss, G.B.; Zagyva, T.; Pásztor, D.; Zaccarini, F. Submarine hydrothermal processes, mirroring the geotectonic evolution of the NE Hungarian Jurassic Szarvaskő Unit. *Int. J. Earth Sci.* **2018**, *107*, 2671–2688. [[CrossRef](#)]
40. Árkai, P.; Faryad, S.W.; Vidal, O.; Balogh, K. Very low-grade metamorphism of sedimentary rocks of the Meliata unit, Western Carpathians, Slovakia: Implications of phyllosilicate characteristics. *Int. J. Earth Sci. (Geol. Rundsch.)* **2003**, *92*, 68–85.
41. Gawlick, H.-J. Triassische Tiefwasserfacieskomponenten (Kieselkalke, Radiolarite) in der jurassischen Strubberg-breckzie am Tennengebirgsnordrand (Nördliche Kalkalpen, Austria). *Jb. Geol. B.-A.* **1993**, *136*, 347–350.
42. Gawlick, H.-J.; Frisch, W. The Middle to late Jurassic carbonate clastic radiolaritic flysch sediments in the Northern Calcareous Alps: Sedimentology, basin evolution, and tectonics—An overview. *Neu. Jb. Geol. Paläont. Abh.* **2003**, *230*, 163–213. [[CrossRef](#)]
43. Bezák, V.; Broska, I.; Ivanička, J.; Reichwalder, P.; Vozár, J.; Polák, M.; Havrila, M.; Mello, J.; Biely, A.; Plašienka, D.; et al. *Tectonic Map of Slovak Republic 1:500,000*; Bezák, V., Ed.; Ministry of the Environment of the Slovak Republic; State Geological Institute of Dionýz Štúr: Bratislava, Slovakia, 2004.

44. Grecula, P.; Kobulský, J.; Gazdačko, L.; Németh, Z.; Hraško, L.; Novotný, L.; Maglay, J. *Geological Map of the Spiš-Gemer Ore Mts. 1:50,000*; Grecula, P., Ed.; Ministry of the Environment of the Slovak Republic; State Geological Institute of Dionýz Štúr: Bratislava, Slovakia, 2009.
45. Putiš, M. Variscan and Alpidic nappe structures of the Western Carpathian crystalline basement. *Geol. Carpath.* **1992**, *43*, 369–380.
46. Németh, Z.; Putiš, M.; Hraško, L. The relation of metallogeny to geodynamic processes - the natural prerequisite for the origin of mineral deposits of public importance (MDoPI): The case study in the Western Carpathians, Slovakia. *Miner. Slov.* **2016**, *48*, 119–134.
47. Putiš, M.; Kotov, A.B.; Uher, P.; Salnikova, E.B.; Korikovskiy, S.P. Triassic age of the Hrončok pre-orogenic A-type granite related to continental rifting: A new result of U-Pb isotope dating (Western Carpathians). *Geol. Carpath.* **2000**, *51*, 59–66.
48. Putiš, M.; Németh, Z.; Li, X.-H.; Yang, Y.-H.; Li, Q.-L.; Ling, X.; Nemeč, O.; Ondrejka, M. Prototethys, Paleotethys and Neotethys remnants in the Western Carpathians constrained by SIMS and LA-ICP-MS U-Pb zircon ages. Geophysical Research Abstracts. In Proceedings of the EGU 2018, Vienna, Austria, 8–13 April 2018.
49. Radvanec, M.; Konečný, P.; Ondrejka, M.; Putiš, M.; Uher, P.; Németh, Z. The Gemeric granites as an indicator of the crustal extension above the Late-Variscan subduction zone and during the Early Alpine riftingogenesis (Western Carpathians): An interpretation from the monazite and zircon ages dated by CHIME and SHRIMP methods. *Miner. Slov.* **2009**, *41*, 381–394, (In Slovak with English summary).
50. Radvanec, M.; Németh, Z.; Král, J.; Pramuka, S. Variscan dismembered metaophiolite suite fragments of Paleo-Tethys in Gemeric unit, Western Carpathians. *Miner. Slov.* **2017**, *49*, 1–48.
51. Frisch, W.; Neubauer, F. Pre-Alpine terranes and tectonic zoning in the Eastern Alps. In *Terranes in the Circum-Atlantic Paleozoic orogens*; Dallmayer, R.D., Ed.; Geological Society of America: Boulder, CO, USA, 1989; pp. 91–100.
52. Neubauer, F.; von Raumer, F.J. The Alpine basement: Linkage between west-European Variscides and Alpine-Mediterranean Mountain Belt. In *The Pre-Mesozoic Geology in the Alps*; Von Raumer, F.J., Neubauer, F., Eds.; Springer: Berlin, Germany, 1993; pp. 640–663.
53. Putiš, M.; Ružička, P.; Ling, X.; Nemeč, O. U/Pb SIMS zircon dating of a rhyolite intercalation in Permian siliciclastics as well as a rhyodacite dyke in micaschists (Infrataticum, W. Carpathians). *Miner. Slov.* **2016**, *48*, 135–144.
54. Spišiak, J.; Vetráková, L.; Chew, D.; Ferenc, Š.; Mikuš, T.; Šimonová, V.; Bačík, P. Petrology and dating of the Permian lamprophyres from the Malá Fatra Mts. (Western Carpathians, Slovakia). *Geol. Carpath.* **2018**, *69*, 453–466. [[CrossRef](#)]
55. Kotov, A.B.; Miko, O.; Putiš, M.; Korikovskiy, S.P.; Salnikova, E.B.; Kovach, V.P.; Yakovleva, S.Z.; Bereznaya, N.G.; Král, J.; Krist, E. U/Pb dating of zircons of postorogenic acid metavolcanics and metasubvolcanics: A record of Permian-Triassic taphrogeny of the West-Carpathian basement. *Geol. Carpath.* **1996**, *47*, 73–79.
56. Vozárová, A.; Rodionov, N.; Vozár, J.; Lepekhina, E.; Šarinová, K. U-Pb zircon ages from Permian volcanic rocks and tonalite of the Northern Veporicum (Western Carpathians). *J. Geosci.* **2016**, *61*, 221–237. [[CrossRef](#)]
57. Vozárová, A.; Šmelko, M.; Paderin, I. Permian single crystal U-Pb zircon ages of the Rožňava Formation volcanites (Southern Gemeric Unit, Western Carpathians, Slovakia). *Geol. Carpath.* **2009**, *60*, 439–448. [[CrossRef](#)]
58. Vozárová, A.; Šmelko, M.; Paderin, I.; Larionov, A. Permian volcanics in the Northern Gemericum and Bôrka Nappe system: U-Pb zircon dating and implication to geodynamic evolution (Western Carpathians, Slovakia). *Geol. Carpath.* **2012**, *63*, 191–200. [[CrossRef](#)]
59. Vozárová, A.; Presnyakov, S.; Šarinová, K.; Šmelko, M. First evidence for Permian-Triassic boundary volcanism in the Northern Gemericum: Geochemistry and U-Pb zircon geochronology. *Geol. Carpath.* **2015**, *66*, 375–391. [[CrossRef](#)]
60. Ondrejka, M.; Li, X.-H.; Vojtko, R.; Putiš, M.; Uher, P.; Sobocký, T. Permian A-type rhyolites of the Muráň Nappe, Inner Western Carpathians, Slovakia: in-situ zircon U-Pb SIMS ages and tectonic setting. *Geol. Carpath.* **2018**, *69*, 187–198. [[CrossRef](#)]
61. Vozárová, A.; Vozár, J. *Late Paleozoic in West Carpathians*; Bratislava, State Geological Institute of Dionýz Štúr: Bratislava, Slovakia, 1988; pp. 1–314.

62. Mello, J.; Ivanička, J.; Grecula, P.; Janočko, J.; Jacko, S.; Elečko, M.; Pristaš, J.; Vass, D.; Polák, M.; Vozár, J.; et al. *General Geological Map of the Slovak Republic, Map sheet: 37—Košice (scale 1:200,000)*; Mello, J., Ivanička, J., Eds.; Ministry of the Environment of the Slovak Republic; State Geological Institute of Dionýz Štúr: Bratislava, Slovakia, 2008.
63. Vozárová, A.; Vozár, J. Tornaicum and Meliaticum in bore-hole Brusník BRU-1, Southern Slovakia (Brusník Anticline, Rimava Depression). *Acta Geol. Acad. Sci. Hung.* **1992**, *35*, 97–116.
64. Mello, J.; Elečko, M.; Pristaš, J.; Reichwalder, P.; Snopko, L.; Vass, D.; Vozárová, A. *Geological Map of the Slovenský Kras Mts., 1:50,000. Regional Geological Maps of Slovakia*; Mello, J., Ed.; Ministry of Environment and State Geological Survey of Slovak Republic: Bratislava, Slovakia, 1996.
65. Lačný, A.; Plašienka, D.; Vojtko, R. Structural evolution of the Turňa Unit constrained by fold and cleavage analyses and its consequences for the regional tectonic models of the Western Carpathians. *Geol. Carpath.* **2016**, *67*, 177–193. [[CrossRef](#)]
66. Biely, A.; Bezák, V.; Elečko, M.; Gross, P.; Kaličiak, M.; Konečný, V.; Lexa, J.; Mello, J.; Nemčok, A.; Potfaj, M.; et al. *Explanation to Geological Map of Slovakia 1: 500,000*; Biely, A., Ed.; GSSR: Bratislava, Slovakia, 1996; pp. 1–77. (In Slovak)
67. Gawlick, H.-J.; Havrila, M.; Krystyn, L.; Lein, R.; Mello, J. Conodont colour alteration indices (CAI) in the Central Western Carpathians and the Northern Calcareous Alps—A comparison. *Geol. Carp.* **2002**, *53*, 15–17.
68. Dumitrică, P.; Mello, J. On the Age of the Meliata Group and the Silica Nappe Radiolarites (localities Držkovce and Bohúňovo, Slovak Karst, ČSSR). *Geol. Práce Spr.* **1982**, *77*, 17–28.
69. Lačný, A.; Józsa, Š.; Ledvényová, L.; Ružička, P. Microfauna from the clasts of the carbonate-silicite breccias found near the Bohúňovo village (Slovak Karst, Western Carpathians). *Miner. Slov.* **2015**, *47*, 189–199. (In Slovak)
70. Ivan, P.; Méres, Š. Blueschist enclave in the Dobšiná serpentinite quarry: The evidence of the relation of the ultrabasic body to the Hačava Fm. of the Bôrka nappe (Meliatic Unit, Slovakia). *Miner. Slov.* **2009**, *41*, 407–418. (In Slovak)
71. Ivan, P.; Méres, Š.; Sýkora, M. Magnesioriebeckite in red cherts and basalts (Jaklovce Fm. of the Meliatic Unit, Western Carpathians): An indicator of initial stage of the high-pressure subduction metamorphism. *Miner. Slov.* **2009**, *41*, 419–432. (In Slovak)
72. Putiš, M.; Radvanec, M.; Sergeev, S.; Koller, F.; Michálek, M.; Snárska, B.; Koppa, M.; Šarinová, K.; Németh, Z. Metamorphosed succession of cherty shales with basalt and diastrophic breccia in olistolith of the Meliatic Jurassic accretion wedge near Jaklovce (Slovakia), dated on zircon (U–Pb SIMS SHRIMP). *Miner. Slov.* **2011**, *43*, 1–18.
73. Putiš, M.; Yang, Y.H.; Koppa, M.; Dyda, M.; Šmál, P. U/Pb LA–ICP–MS age of metamorphic-metasomatic perovskite from serpentinitized harzburgite in the Meliata Unit at Dobšiná, Slovakia: Time constraint of fluid-rock interaction in an accretionary wedge. *Acta Geol. Slov.* **2015**, *7*, 63–71.
74. Leško, B.; Varga, I. Alpine elements in the West Carpathian structure and their significance. *Miner. Slov.* **1980**, *12*, 97–130.
75. Faryad, S.W. Lithology and metamorphism of the Meliata unit high-pressure rocks. In *Geological Evolution of the Western Carpathians*; Grecula, P., Hovorka, D., Putiš, M., Eds.; Mineralia Slovaca: Bratislava, Slovakia, 1997; pp. 1–24.
76. Plašienka, D.; Méres, Š.; Ivan, P.; Sýkora, M.; Soták, J.; Lačný, A.; Aubrecht, R.; Bellová, S.; Potočný, T. Meliatic blueschists and their detritus in Cretaceous sediments: New data constraining tectonic evolution of the West Carpathians. *Swiss J. Geosci.* **2018**, *112*, 55–81. [[CrossRef](#)]
77. Kozur, H.; Mock, R. New paleogeographic and tectonic interpretations in the Slovakian Carpathians and their implications for correlations with the Eastern Alps and other parts of the Western Tethys. Part II: Inner Western Carpathians. *Miner. Slov.* **1997**, *29*, 164–209.
78. Mazzoli, C.; Sassi, R.; Vozárová, A. *The Pressure Character of the Alpine Metamorphism in the Central and Inner Western Carpathians (Czecho-Slovakia)*; Vozár, J., Ed.; D. Štúr Inst. Geol.: Bratislava, Slovakia, 1992; Special volume IGCP; pp. 109–117.
79. Faryad, S.W.; Hoinkes, G. Two Contrasting Mineral Assemblages in the Meliata Blueschists, Western Carpathians, Slovakia. *Miner. Mag.* **1999**, *63*, 489–501. [[CrossRef](#)]

80. Dallmeyer, R.D.; Neubauer, F.; Putiš, M.  $^{40}\text{Ar}/^{39}\text{Ar}$  mineral age controls for the Pre-Alpine and Alpine tectonic evolution of nappe complexes in the Western Carpathians. In *Pre-Alpine Events in the Western Carpathians' Realm*; Pitoňák, P., Spišiak, J., Eds.; Confer. excur. guide; Slovak Academy of Sciences: Bratislava, Slovakia, 1993; pp. 11–20.
81. Dallmeyer, R.D.; Neubauer, F.; Handler, R.; Fritz, H.; Müller, W.; Pana, D.; Putiš, M. Tectonothermal evolution of the internal Alps and Carpathians: Evidence from  $^{40}\text{Ar}/^{39}\text{Ar}$  mineral and whole-rock data. *Eclogae Geol. Helv.* **1996**, *89*, 203–227.
82. Dallmeyer, R.D.; Németh, Z.; Putiš, M. Regional tectonothermal events in Gemericum and adjacent units (Western Carpathians, Slovakia): Contribution by the  $^{40}\text{Ar}/^{39}\text{Ar}$  dating. *Slovak Geol. Mag.* **2005**, *11*, 155–163.
83. Maluski, H.; Rajlich, P.; Matte, P.  $^{40}\text{Ar}$ - $^{39}\text{Ar}$  dating of the Inner Carpathians Variscan basement and Alpine mylonitic overprinting. *Tectonophysics* **1993**, *223*, 313–337. [[CrossRef](#)]
84. Faryad, S.W.; Henjes-Kunst, F. Petrological and K–Ar and  $^{40}\text{Ar}$ - $^{39}\text{Ar}$  age constraints for the tectonothermal evolution of the high-pressure Meliata unit, Western Carpathians (Slovakia). *Tectonophysics* **1997**, *280*, 141–156. [[CrossRef](#)]
85. Kozur, H.; Mock, R.; Ožvoldová, L. New biostratigraphic results in the Meliaticum in its type area around Meliata village (Slovakia) and their tectonic and paleogeographic significance. *Geol. Paläont. Mitt. Innsbruck* **1996**, *21*, 89–121.
86. Németh, Z.; Radvanec, M.; Kobulský, J.; Gazdačko, L.; Putiš, M.; Zákršmidová, B. Allochthonous position of the Meliaticum in the North-Gemeric zone (Inner Western Carpathians) as demonstrated by paleopiezometric data. *Miner. Slov.* **2012**, *44*, 57–64.
87. Árkai, P.; Kovács, S. Diagenesis and regional metamorphism of Aggtelek - Rudabánya Mountains (Northern Hungary). *Acta Geol. Hungarica* **1986**, *29*, 349–373.
88. Plašienka, D.; Broska, I.; Kissová, D.; Dunkl, I. Zircon fission-track dating of granites from the Vepor-Gemer Belt (Western Carpathians): Constraints for the Early Alpine exhumation history. *J. Geosci.* **2007**, *52*, 113–123. [[CrossRef](#)]
89. Vojtko, R.; Králiková, S.; Jeřábek, P.; Schuster, R.; Danišík, M.; Fügenschuh, B.; Minár, J.; Madarás, J. Geochronological evidence for the Alpine tectono-thermal evolution of the Veporic Unit (Western Carpathians, Slovakia). *Tectonophysics* **2016**, *666*, 48–65. [[CrossRef](#)]
90. Putiš, M.; Yang, Y.-H.; Vaculovič, T.; Koppa, M.; Li, X.-H.; Uher, P. Perovskite, reaction product of a harzburgite with Jurassic–Cretaceous accretionary wedge fluids (Western Carpathians, Slovakia): Evidence from the whole-rock and mineral trace element data. *Geol. Carpath.* **2016**, *67*, 133–146. [[CrossRef](#)]
91. Koppa, M.; Koller, F.; Putiš, M. Petrology and geochemistry of a peridotite body in Central Carpathian Paleogene sediments (Sedlice, eastern Slovakia). *Geol. Carpath.* **2014**, *65*, 387–399. [[CrossRef](#)]
92. Li, X.-H.; Putiš, M.; Yang, Y.-H.; Koppa, M.; Dyda, M. Accretionary wedge harzburgite serpentinization and rodingitization constrained by perovskite U/Pb SIMS age, trace elements and Sm/Nd isotopes: Case study from the Western Carpathians, Slovakia. *Lithos* **2014**, *205*, 1–14. [[CrossRef](#)]
93. Kamenetsky, V.; Crawford, A.J.; Meffre, S. Factors controlling chemistry of magmatic spinel: An empirical study of associated olivine, Cr-spinel and melt inclusions from primitive rocks. *J. Petrol.* **2001**, *42*, 655–671. [[CrossRef](#)]
94. Choi, S.H.; Shervais, J.W.; Mukasa, S.B. Supra-subduction and abyssal mantle peridotites of the Coast Range ophiolite, California. *Contrib. Miner. Petr.* **2008**, *156*, 551–576. [[CrossRef](#)]
95. Li, X.-H.; Liu, Y.; Li, Q.-L.; Guo, C.H.; Chamberlain, K.R. Precise determination of Phanerozoic zircon Pb/Pb age by multi-collector SIMS without external standardization. *Geochem. Geophys. Geosyst.* **2009**, *10*, 1–21.
96. Li, Q.L.; Lin, W.; Su, W.; Li, X.H.; Shi, Y.H.; Liu, Y.; Tang, G.Q. SIMS U–Pb rutile age of low-temperature eclogites from Southwestern Chinese Tianshan, NW China. *Lithos* **2011**, *122*, 76–86. [[CrossRef](#)]
97. Sláma, J.; Košler, J.; Condon, D.J.; Crowley, J.L.; Gerdes, A.; Hanchar, J.M.; Horstwood, M.S.A.; Morris, G.A.; Nasdala, L.; Norberg, N.; et al. Plešovice zircon—A new natural reference material for U–Pb and Hf isotopic microanalysis. *Chem. Geol.* **2008**, *249*, 1–353. [[CrossRef](#)]
98. Wiedenbeck, M.; Alle, P.; Corfu, F.; Griffin, W.L.; Meier, M.; Oberli, F.; Vonquadt, A.; Roddick, J.C.; Speigel, W. Three natural zircon standards for U–Th–Pb, Lu–Hf, trace-element and REE analyses. *Geostand. Newsl.* **1995**, *19*, 1–23. [[CrossRef](#)]

99. Li, X.H.; Tang, G.Q.; Gong, B.; Yang, Y.H.; Hou, K.J.; Hu, Z.C.; Li, Q.L.; Liu, Y.; Li, W.X. Qinghu zircon: A working reference for microbeam analysis of U-Pb age and Hf and O isotopes. *Chin. Sci. Bull.* **2013**, *58*, 4647–4654. [[CrossRef](#)]
100. Ludwig, K.R. *User's Manual for Isoplot/Ex rev. 2.49. A Geochronological Toolkit for Microsoft Excel*; Berkeley Geochronology Centre Special Publication: Berkeley, CA, USA, 2001; Volume 1, p. 56.
101. Li, C.F.; Li, X.-H.; Li, Q.-L.; Guo, J.H.; Yang, Y.-H. Rapid and precise determination of Sr and Nd isotopic ratios in geological samples from the same filament loading by thermal ionization mass spectrometry employing a single-step separation scheme. *An. Chim. Acta* **2012**, *727*, 54–60. [[CrossRef](#)] [[PubMed](#)]
102. Kozur, H.; Mostler, H. Anisian to Middle Carnian radiolarian zonation and description of some stratigraphically important radiolarians. *Geol. Paläont. Mitt. Innsbr. Sonderbd.* **1994**, *3*, 39–255.
103. Halamić, J.; Goričan, Š. Triassic Radiolarites from Mts. Kalnik and Medvednica (Northwestern Croatia). *Geol. Croat.* **1995**, *48*, 129–146.
104. Gawlick, H.-J.; Frisch, W.; Hoxha, L.; Dumitrică, P.; Krystyn, L.; Lein, R.; Missoni, S.; Schlagintweit, F. Mirdita Zone ophiolites and associated sediments in Albania reveal Neotethys Ocean origin. *Int J. Earth Sci. (Geol. Rundsch.)* **2008**, *97*, 865–881. [[CrossRef](#)]
105. Oszvárt, P.; Kovács, S. Revised Middle and Late Triassic radiolarian ages for ophiolite mélanges: Implications for the geodynamic evolution of the northern part of the early Mesozoic Neotethyan subbasins. *Bull. Soc. Géol. France* **2012**, *183*, 273–286. [[CrossRef](#)]
106. O'Dogherty, L.; Carter, E.S.; Goričan, Š.; Dumitrică, P. Triassic radiolarian biostratigraphy. In *The Triassic Time Scale*; Lucas, S.G., Ed.; The Geological Society of London: London, UK, 2010; Volume 334, pp. 163–200.
107. Pearce, J.A. A user's guide to basalt discrimination diagrams. In *Trace Element Geochemistry of Volcanic Rocks; Applications for Massive Sulphide Exploration*; Short Course Notes; Wyman, D.A., Ed.; Geological Association of Canada: Winnipeg, MB, Canada, 1996; Volume 12, pp. 79–113.
108. Wood, D.A. The application of a Th-Hf-Ta diagram to problems of tectonomagmatic classification and to establishing the nature of crustal contamination of basaltic lavas of the British Tertiary volcanic province. *Earth Planet. Sci. Lett.* **1980**, *50*, 11–30. [[CrossRef](#)]
109. Pearce, J.A. Geochemical fingerprinting of oceanic basalts with applications to ophiolite classification and the search for Archean oceanic crust. *Lithos* **2008**, *100*, 14–48. [[CrossRef](#)]
110. Cabanis, B.; Lecolle, M. Le diagramme La/10-Y/15-Nb/8: Un outil pour la discrimination des séries volcaniques et la mise en évidence des processus de mélange et/ou de contamination crustale. *Comptes Rendus De L'Academie Des Sci. Paris Ser. 2* **1989**, *313*, 2023–2029. (In French)
111. Meschede, M. A method of discrimination between different types of mid-ocean ridge basalts and continental tholeiites with the Nb–Zr–Y diagram. *Chem. Geol.* **1986**, *56*, 207–218. [[CrossRef](#)]
112. McDonough, W.F.; Sun, S.-S.; Ringwood, A.E.; Jagoutz, E.; Hofmann, A.W. Potassium, Rubidium and Cesium in the Earth and Moon and the evolution of the mantle of the Earth. *Geochim. Cosmochim. Acta* **1992**, *56*, 1001–1012. [[CrossRef](#)]
113. Shervais, J.W. Ti-V plots and the petrogenesis of modern ophiolitic lavas. *Earth Planet. Sci. Lett.* **1982**, *59*, 101–118. [[CrossRef](#)]
114. Pearce, J.A. Immobile Element Fingerprinting of Ophiolites. *Elements* **2014**, *10*, 101–108. [[CrossRef](#)]
115. Pearce, J.A. Role of the sub-continental lithosphere in magma genesis at active continental margins. In *Continental Basalts and Mantle Xenoliths*; Hawkesworth, C.J., Norry, M.J., Eds.; Shiva Publications: Nantwich, UK, 1983; pp. 230–249.
116. McDonough, W.F.; Sun, S. The composition of the Earth. *Chem. Geol.* **1995**, *120*, 223–253. [[CrossRef](#)]
117. Gale, A.; Dalton, C.A.; Langmuir, C.H.; Su, Y.; Schilling, J.-G. The mean composition of ocean ridge basalts. *Geochem. Geophys. Geosyst.* **2013**, *14*, 489–518. [[CrossRef](#)]
118. Faryad, S.W. Glaucophanized amphibolites and gneisses near Rudník (Gemicum). *Geol. Zbor. Geol. Carp.* **1988**, *39*, 747–763.
119. Putiš, M.; Frank, W.; Plašienka, D.; Siman, P.; Sulák, M.; Biroň, A. Progradation of the Alpidic Central Western Carpathians orogenic wedge related to two subductions: Constrained by  $^{40}\text{Ar}/^{39}\text{Ar}$  ages of white micas. *Geodin. Acta* **2009**, *22*, 31–56. [[CrossRef](#)]
120. Pearce, J.A. Trace element characteristics of lavas from destructive plate boundaries. In *Andesites: Orogenic Andesites and Related Rocks*; Thorpe, R.S., Ed.; John Wiley and Sons: Hoboken, NJ, USA, 1982; pp. 252–548.

121. Sun, S.-s.; McDonough, W.F. Chemical and isotopic systematics of oceanic basalts: Implications for mantle composition and processes. *Geol. Soc. London Spec. Publ.* **1989**, *42*, 313–345. [[CrossRef](#)]
122. Saccani, E.; Dilek, Y.; Marroni, M.; Pandolfi, L. Continental margin ophiolites of Neotethys: Remnants of Ancient Ocean–Continent Transition Zone (OCTZ) lithosphere and their geochemistry, mantle sources and melt evolution patterns. *Episodes J. Int. Geosci.* **2015**, *38*, 230–249. [[CrossRef](#)]
123. Pearce, J.A.; Peate, D.W. Tectonic implications of the composition of volcanic arc magmas. *Annu. Rev. Earth Planet. Sci.* **1995**, *23*, 251–285. [[CrossRef](#)]
124. Pe-Piper, G. The nature of Triassic extension-related magmatism in Greece: Evidence from Nd and Pb isotope geochemistry. *Geol. Mag.* **1998**, *135*, 331–348. [[CrossRef](#)]
125. Saccani, E.; Photiades, A. Petrogenesis and tectono-magmatic significance of volcanic and subvolcanic rocks in the Albanide-Hellenide ophiolitic mélanges. *Island Arc* **2005**, *14*, 494–516. [[CrossRef](#)]
126. Bortolotti, V.; Chiari, M.; Kodra, A.; Martucci, M.; Marroni, M.; Mustafa, F.; Prella, M.; Pandolfi, L.; Principi, G.; Saccani, E. Triassic MORB magmatism in the southern Mirdita zone (Albania). *Ofioliti* **2006**, *31*, 1–9.
127. Bortolotti, V.; Chiari, M.; Marcucci, M.; Photiades, A.; Principi, G.; Saccani, E. New geochemical and age data on the ophiolites from the Othrys area (Greece): Implication for the Triassic evolution of the Vardar ocean. *Ofioliti* **2008**, *33*, 135–151.
128. Bortolotti, V.; Chiari, M.; Marroni, M.; Pandolfi, L.; Principi, G.; Saccani, E. Geodynamic evolution of the ophiolites from Albania and Greece (Dinaric-Hellenic belt). One, two or more oceanic basins? *Int J. Earth Sci.* **2013**, *102*, 783–811. [[CrossRef](#)]
129. Uysal, İ.; Ersoy, E.Y.; Karşlı, O.; Dilek, Y.; Sadıklar, M.B.; Ottley, C.J.; Tiepolo, M.; Meisel, T. Coexistence of abyssal and ultra-depleted SSZ type mantle peridotites in a Neo-Tethyan Ophiolite in SW Turkey: Constraints from mineral composition, whole-rock geochemistry (major–trace–REE–PGE), and Re–Os isotope systematics. *Lithos* **2012**, *132–133*, 50–69. [[CrossRef](#)]
130. Furnes, H.; Dilek, Y. Geochemical characterization and petrogenesis of intermediate to silicic rocks in ophiolites: A global synthesis. *Earth-Sci. Rev.* **2017**, *166*, 1–37. [[CrossRef](#)]
131. Le Bas, M.J.; Le Maitre, R.W.; Streckeisen, A.; Zanettin, B. A chemical classification of volcanic rocks based on the total alkali-silica diagram. *J. Petrol.* **1986**, *27*, 745–750. [[CrossRef](#)]
132. Hovorka, D. Keratophyres in the Triassic near Jaklovce (Spišsko-gemerské rudohorie Mts—West Carpathians). *Acta Geol. Et Geogr. Univ. Comen. Geol.* **1977**, *32*, 57–79. (In Slovak)
133. Mello, J.; Vozárová, A.; Vozár, J.; Gargulák, M.; Hanzel, V.; Káčer, Š.; Karoli, S.; Molák, B.; Šucha, V.; Siráňová, V. *Report on Structural Borehole Držkovce (DRŽ-1)*; Archive of D. Štúr Inst. Geol.: Bratislava, Slovakia, 1994. (In Slovak)
134. Mundil, R.; Brack, P.; Meier, M.; Rieber, H.; Oberli, F. High resolution U–Pb dating of Middle Triassic volcanics: Time-scale calibration and verification of tuning parameters for carbonate sedimentation. *Earth Planet. Sci. Lett.* **1996**, *141*, 137–151. [[CrossRef](#)]
135. Dunkl, I.; Farics, É.; Józsa, S.; Lukács, R.; Haas, J.; Budai, T. Traces of Carnian volcanic activity in the Transdanubian Range, Hungary. *Int. J. Earth Sci.* **2019**, *108*, 1451–1466. [[CrossRef](#)]
136. Everard, J.L. A blue amphibole occurrence from the Flowerdale River, northern Arthur Lineament. *Miner. Resour. (Geol. Surv. Tasmania)* **1999**, *5*, 117.
137. Hawthorne, F.C.; Oberti, R.; Harlow, G.E.; Maresch, W.V.; Martin, R.F.; Schumacher, J.C.; Welch, M.D. Nomenclature of the amphibole supergroup. *Am. Miner.* **2012**, *97*, 2031–2048. [[CrossRef](#)]
138. Tischendorf, G.; Förster, H.-J.; Gottesmann, B.; Rieder, M. True and brittle micas: Composition and solid-solution series. *Miner. Mag.* **2007**, *71*, 285–320. [[CrossRef](#)]

